Alternative splicing downstream of EMT enhances phenotypic plasticity and malignant behaviour in colon cancer.

Tong Xu[1], Mathijs Verhagen[1], Rosalie Joosten[1], Wenjie Sun[2], Andrea Sacchetti[1], Leonel Munoz Sagredo[3,4], Véronique Orian-Rousseau[4], and Riccardo Fodde[1*]

[1]Department of Pathology, Erasmus University Medical Center, Rotterdam, The Netherlands. [2]Institut Curie, Laboratory of Genetics and Developmental Biology, Paris, France. [3]Faculty of Medicine, University of Valparaiso, Chile; [4]Institute of Biological and Chemical Systems - Functional Molecular Systems (IBCS-FMS), Karlsruhe Institute of Technology (KIT), Germany.

*to whom correspondence should be addressed at:

Erasmus MC, Department of Pathology, PO Box 2040, 3000 CA Rotterdam, The Netherlands

E-mail: r.fodde@erasmusmc.nl Tel: +31 10 7043896

Running title: *Colon cancer metastasis controlled by alternative splicing*

Keywords: EMT, RNA-binding proteins, ESRP1, CD44, NUMB

Competing interest statement: *The authors declare no competing interests*.

Abstract

Phenotypic plasticity allows carcinoma cells to transiently acquire the quasi-mesenchymal features necessary to detach from the primary mass and proceed along the invasion-metastasis cascade. A broad spectrum of epigenetic mechanisms is likely to cause the epithelial–to-mesenchymal (EMT) and mesenchymal-to-epithelial (MET) transitions necessary to allow local dissemination and distant metastasis. Here, we report on the role played by alternative splicing (AS) in eliciting phenotypic plasticity in epithelial malignancies with focus on colon cancer.

By taking advantage of the coexistence of subpopulations of fully epithelial ($EpCAM^{hi}$) and quasi-mesenchymal and highly metastatic ($EpCAM^{lo}$) cells in conventional human cancer cell lines, we here show that the differential expression of *ESRP1* and other RNA-binding proteins (RBPs) downstream of the EMT master regulator *ZEB1*, alters the AS pattern of a broad spectrum of targets including *CD44* and *NUMB*, thus resulting in the generation of specific isoforms functionally associated with increased invasion and metastasis. Additional functional and clinical validation studies indicate that both the newly identified RBPs and the CD44s and NUMB2/4 splicing isoforms promote local invasion and distant metastasis and are associated with poor survival in colon cancer.

The systematic elucidation of the spectrum of EMT-related RBPs and AS targets in epithelial cancers, apart from the insights in the mechanisms underlying phenotypic plasticity, will lead to the identification of novel and tumor-specific therapeutic targets.

Introduction

Colon cancer still represents one of the major causes of cancer-related morbidity and mortality worldwide. Apart from its high incidence, the adenoma-carcinoma sequence along which colon cancer progresses has served as a classic model to elucidate the underlying genetic alterations representative of virtually all of the hallmarks of cancers[1], possibly with the only exception of "*activating invasion and metastasis (unlocking phenotypic plasticity; non-mutational epigenetic reprogramming)*". As also reported in other epithelial cancers, the several steps of the invasion-metastasis cascade are not caused by genetic alterations but rather by transient morphological and gene expression changes of epigenetic nature[2,3]. In this context, epithelial–mesenchymal transition (EMT), and its reverse MET, likely represent the main mechanisms underlying local dissemination and distant metastasis[4,5]. EMT is triggered at the invasive front of the primary colon carcinoma in cells earmarked by nuclear β-catenin and enhanced Wnt signaling, as the result of their physical and paracrine interactions with the microenvironment[6]. The acquisition of quasi-mesenchymal features allows local invasion and dissemination through the surrounding stromal compartment. Of note, EMT/MET should not be regarded as binary processes in view of the existence of metastable hybrid E/M states (partial EMT or pEMT) endowed with phenotypic plasticity and likely to underlie the reversible morphological and functional transitions necessary to successfully complete the invasion-metastasis cascade[7].

The molecular basis of the epigenetic changes underlying EMT and MET is likely to encompass a broad spectrum of mechanisms ranging from chromatin remodeling and histone modifications to promoter DNA methylation, non-coding RNAs (e.g. micro RNAs), and alternative splicing (AS). The inclusion/exclusion of specific exons in mature mRNAs results in different protein isoforms with distinct biological functions. AS occurs in 92–94% of human genes leading to enriched protein density[8,9]. Several sequence-specific RNA-binding proteins (RBPs) have been identified which bind pre-mRNAs to control AS in context-dependent fashion[10]. Multiple cancer-specific AS variants have been found to underlie

63 progression and metastasis[11]. Likewise, alternative splicing has been suggested to play key roles in
64 EMT/MET[12,13] and phenotypic plasticity[14] in cancer by expression changes in RBP-encoding genes and
65 their consequences for the modulation of downstream AS targets.
66 The *ESRP1* (epithelial splicing regulatory protein 1) gene encodes for an epithelial-specific RBP and
67 splicing regulator shown to play a central role in EMT by modulating AS of EMT-associated genes
68 including *FGFR2*, Mena, *CD44* and p120-catenin[4]. Relevant to the present study, ESRP1 was reported to
69 regulate the EMT transition from CD44v (variable) to CD44s (standard) isoforms in breast and lung
70 cancer progression[15,16]. As for colon cancer, whether ESRP1 regulates alternative splicing of CD44 and
71 other target genes downstream of EMT/MET activation during invasion and metastasis, is yet poorly
72 understood.
73 Recently, we identified and thoroughly characterized subpopulations of $CD44^{hi}$/$EpCAM^{lo}$ cells (here
74 referred to as $EpCAM^{lo}$) that coexist within immortalized colon cancer cell lines with their epithelial
75 counterparts ($CD44^{hi}$/$EpCAM^{hi}$; for brevity $EpCAM^{hi}$) through stochastic state transitions governed by
76 phenotypic plasticity and pEMT[17]. Accordingly, $EpCAM^{lo}$ cells feature highly invasive and metastatic
77 capacities. Here, we took advantage of these *in vitro* models of phenotypic plasticity to test the
78 hypothesis according to which alternative splicing driven by upstream RBPs underlie epithelial to
79 mesenchymal (and mesenchymal to epithelial) transitions. Among the identified AS targets, specific
80 CD44 and NUMB isoforms were shown to paly specific and unexpected roles in stemness and cancer.
81 Moreover, we provide an extensive list of additional EMT-related RBPs and AS targets and show that
82 many are conserved in other epithelial malignancies. Likewise, RBPs and AS targets differentially
83 expressed among distinct carcinoma types are likely to reflect the distinct modalities through which
84 these malignant cells metastasize.
85

Results

Differential expression of RNA-binding proteins in the quasi-mesenchymal and highly metastatic EpCAM^{lo} colon cancer cells affects alternative splicing of a broad spectrum of downstream target genes.

As previously reported, the EpCAM^{lo} subpopulation of colon cancer cells is earmarked by increased expression of the *ZEB1* transcription factor, responsible for EMT activation and for their quasi-mesenchymal and highly metastatic phenotype[17]. It has been established that in breast and pancreatic cancer *ZEB1*-driven EMT downregulates the expression of the RNA-binding protein and splicing regulator *ESRP1* as part of a self-enforcing feedback loop[24]. Accordingly, among the top differentially expressed genes between EpCAM^{lo} and EpCAM^{hi} in SW480 and HCT116 colon cancer cells, *ESRP1* was found to be downregulated both at the RNA and protein level in the quasi-mesenchymal subpopulation where *ZEB1* expression is upregulated (Figure 1A-C). Gain- and loss-of-function analyses of both genes confirmed the inter-dependence of their expression levels in both cell lines (Figure 1D-E). Of note, *ESRP1*-overexpression in the HCT116 and SW480 cell lines resulted in the dramatic reduction of their EpCAM^{lo} subpopulations and the expansion of the epithelial bulk (EpCAM^{hi}), as shown by FACS analysis (Figure 1F, Figure 1-figure supplement 1A). However, *ESRP1* knockdown (KD) gave rise to less clear and extremely variable results among the individual clones analyzed by FACS, in particular in the SW480 cell line. More coherent and representative result were obtained with the pools of the KD transfections (Figure 1-figure supplement 1B).

These results suggest that RNA binding proteins other than ESRP1 are likely to be involved in the alternative splicing regulation of the EpCAM^{lo} colon cancer subpopulation. Indeed, by taking advantage of the RBPDB database[25], we found that, apart from *ESRP1*, consistent differential expression in the quasi-mesenchymal subpopulation of both cell lines was observed for *ESRP2*, *RBM47*, *MBNL3* (down-

regulated) and *NOVA2*, *MBNL2*, (up-regulated). Other RBPs were found to be differentially expressed though in only one of the two cell lines (Figure 1-figure supplement 1C). In validation of the clinical relevance of the RBPs found to be differential expressed between the EpCAM$^{hi/lo}$ subpopulations derived from the SW480 and HCT116 cell lines, the RBP-coding genes *QKI*, *RBM24*, and *MBNL2* (up in EpCAM^{lo}), and *ESRP1/2* and *RBM47* (down in EpCAM^{lo}) were found to be respectively up- and down-regulated in the consensus molecular subtype 4 (CMS4) of colon cancers, responsible for ~25% of the cases and earmarked by poor prognosis and a pronounced mesenchymal component (Figure 1-figure supplement 1D)[22].

Differentially spliced target genes between EpCAM^{lo} and EpCAM^{hi} colon cancer cells from the SW480 and HCT116 cell lines were selected based on exon skip splicing events with ΔPSI (differential Percentage Spliced In) values > 10%. The PSI value ranges from 0 to 1 and is a measurement of the percentage of isoform with an alternative exon included[26]. This resulted in a large and rather heterogeneous group of alternative spliced targets (n=1495; Supplementary File 1a) with no clear enrichment in any specific gene ontology class (data not shown). In order to identify differentially spliced target genes in RBP-specific fashion, we took advantage of RNAseq data sets from previous *ESRP1*-, *ESRP2*-, *RBM47*-, and *QKI*-knockdown studies in different cancer cell lines and compared them with our own AS data relative to the EpCAM$^{hi/lo}$ colon cancer subpopulations[17] (Figure 2A and Figure 2-figure supplement 1). A total of 32 common skipped exons events in 20 genes were identified between EpCAM^{lo} colon (both cell lines) and *ESRP1* KD H358 lung cancer cells[18] (Figure 2A). More extensive lists of common *ESRP1* AS events and target genes were obtained when the SW480 and HCT116 cell lines were individually compared with the lung cancer study (Supplementary File 1B-C). As for the alternative splicing targets of RBPs other than *ESRP1*, based on the available RNAseq data from knockdown studies of *ESRP2* (in the LNCaP cell line[19]), *RBM47* (H358[18]), and *QKI* (CAL27; GEO Accession: GSM4677985), several common and unique genes were found (Figure 2-figure supplement 1 and Supplementary File 2).

133 Notably, four EMT-related genes (*CTNND1*[27], *LSR*[28], *SLK*[29], and *TCF7L2*[30]) were common to all RBP KD
134 studies analyzed (Figure 2-figure supplement 1).
135
136 ***The CD44s and NUMB2/4 ESRP1-specific AS isoforms are preferentially expressed in EpCAM^{lo} colon***
137 ***cancer cells.***
138 From the newly generated lists of RBP-specific alternative splicing targets, we selected *CD44* and
139 *NUMB* for further analysis, based both on their *ESRP1*-specific AS patterns and on their well-established
140 roles in EMT, stemness/differentiation, and cancer progression.
141 CD44, a transmembrane cell surface glycoprotein, has been show to play key roles in inflammatory
142 responses and in cancer metastasis[31]. The *CD44* gene encompasses 20 exons of which 1-5 and 16-20 are
143 constant and exist in all isoforms. In contrast, exons 6-14, also referred to as variants exons v2-v10, are
144 alternatively spliced and often deregulated in cancer[31]. The *NUMB* gene and its protein product have
145 been involved in a broad spectrum of cellular phenotypes including cell fate decisions, maintenance of
146 stem cell niches, asymmetric cell division, cell polarity, adhesion, and migration. In cancer, NUMB is a
147 tumor suppressor that regulates, among others, Notch and Hedgehog signaling[32]. The mammalian
148 *NUMB* gene encodes for 4 isoforms, ranging from 65 to 72 KD, differentially encompassing two key
149 functional domains, i.e. the amino-terminal phosphotyrosine-binding (PTB) domain, and a C-terminal
150 proline-rich region (PRR) domain[32].
151 Based on the above ΔPSI-based AS analysis, decreased expression of CD44v (variable) isoforms was
152 observed in EpCAM^{lo} and *ESRP1*-KD cells, accompanied by increased CD44s (standard) isoform
153 expression (Figure 2B). Likewise, the NUMB2/4 isoforms appear to be preferentially expressed in
154 EpCAM^{lo} and *ESRP1*-KD, accompanied by decreased NUMB1/3 expression (Figure 2B , Suppl Figure 2B).
155 RTqPCR and western analyses validated these *in silico* data: CD44s and NUMB2/4 isoforms were
156 preferentially expressed in EpCAM^{lo} colon cancer cells, in contrast with the increased CD44v and

NUMB1/3 levels in EpCAM^{hi} cells (Figure 2C-D). In view of its previously suggested role in invasion and metastasis[33], we focused on the CD44v6 isoform.

As reported above, AS events at the *NUMB* and *CD44* genes correlate with decreased ESRP1 expression. To confirm this observation, we up- and down-regulated *ESRP1* in the SW480 and HCT116 cell lines. The dox-inducible shRNA vector used for the KD studies reduces ESRP1 expression by 5-10 fold (Figure 1D-E) and resulted in the upregulation of the CD44s and NUMB2/4 isoforms at the mRNA and protein level in both cell lines (Figure 3A-B and Figure 3-figure supplement 1A-B). Likewise, *ESRP1* overexpression led to an increase in the CD44v6 and NUMB1/3 isoforms, found in association with the bulk of epithelial colon cancer cells (Figure 3C-D and Figure 3-figure supplement 1C-D).

Transcriptional and functional consequences of the CD44s and NUMB2/4 isoforms on colon cancer invasion and metastasis.

In order to elucidate the functional contribution exerted by the newly identified CD44s and NUMB2/4 isoforms on the overall invasive and metastatic capacities of colon cancer cells, we first ectopically expressed each of them (individually and in combination for NUMB1/3 and 2/4) in the HCT116 and SW480 cell lines (Figure 3-figure supplement 1E-H), and analyzed their consequences *in vitro* by cell proliferation, transwell migration assay, RTqPCR, western, FACS, and RNAseq, and *in vivo* by spleen transplantation. A significant increase in migratory capacity (Figure 3-figure supplement 2A-B), comparable to that of EpCAM^{lo} cells sorted from the parental lines, was observed in SW480 and HCT116 upon overexpression of the CD44s and NUMB2/4 isoforms (Figure 3-figure supplement 2A-B). Likewise, ectopic expression of the single NUMB2 or 4 isoforms resulted in increased migration rates when compared with NUMB1 and 3. In contrast, overexpression of CD44v6 and NUMB1/3, normally prevalent in the epithelial bulk (EpCAM^{hi}) of both cell lines, did not affect their migratory properties (Figure 3-figure supplement 2A-B).

In agreement with the migration assays, overexpression of CD44s and NUMB2/4 results in the significant upregulation of the EMT transcription factors (EMT-TFs) *ZEB1*, accompanied by the up- and downregulation regulation of mesenchymal and epithelial markers such as *VIM* (vimentin), *CDH1* (E-cadherin), and *EpCAM*, respectively (Figure 3-figure supplement 2C). Of note, expression of *ESRP1*, the main upstream splicing regulator of both CD44 and NUMB, was also decreased in CD44s- and NUMB2/4-OE cells, in confirmation of the self-enforcing feedback loop that characterize its interaction with ZEB1 and EMT activation[24]. In agreement with the well-established regulation of Notch signaling by NUMB isoforms[32], established Notch target genes and were accordingly up- (*HES1*, *HEY1*) and down-regulated (*ID2*) upon overexpression of NUMB2/4 (Figure 3-figure supplement 2D).

FACS analysis was then employed to evaluate the overall effect of the ectopic expression of the specific CD44 and NUMB isoforms on the relative percentages of the $EpCAM^{hi/lo}$ subpopulations in the HCT116 and SW480 cell lines. As shown in Figure 4A, CD44s overexpression led to a dramatic increase of the $EpCAM^{lo}$ subpopulation at the expenses of $EpCAM^{hi}$ cells. The opposite effect was observed with CD44v6, i.e. the enlargement of the $EpCAM^{hi}$ gate and the corresponding decrease of $EpCAM^{lo}$ cells. As for NUMB, ectopic expression of NUMB2/4 significantly increased the relative proportion of $EpCAM^{lo}$ cells while reducing the size of the $EpCAM^{hi}$ subpopulation, while the opposite was observed with NUMB1/3 (Figure 4B-C). Of note, the single NUMB2 and NUMB4 isoforms appear dominant in their capacity to enlarge the HCT116 and SW480 $EpCAM^{lo}$ subpopulations, respectively. The same was true for NUMB1 and NUMB3 in the consequences of their ectopic expression in reducing the size of the HCT116 and SW480 $EpCAM^{lo}$ fractions, respectively (Figure 4B-C). In agreement with the RTqPCR analysis of EMT markers, CD44s overexpression negatively affected overall proliferation rates in both cell lines, whereas the opposite was observed upon CD44v6 expression (Figure 4-figure supplement 1A-B). Likewise, NUMB1/3 expression positively affected proliferation rates in HCT116 and SW480, whereas the NUMB2/4 isoforms

exert the opposite effects. In both cases, synergistic effects were observed upon co-expression of NUMB1/3 and 2/4, when compared to the individual isoforms (Figure 4-figure supplement 1C-D).

In order to assess the *in vivo* the consequences of the ectopic expression of the CD44 and NUMB isoforms on the capacity of colon cancer cells to form metastatic lesions in the liver, parental HCT116 and SW480 cells and their CD44s-, CD44v6-, NUMB1/3-, and NUMB1/4-overexpressing counterparts were injected in the spleen of immune-incompetent recipient mice. In agreement with the *in vitro* results, overexpression of both NUMB2/4 and CD44s isoforms significantly increased the multiplicity of liver metastases, whereas CD44v6 and NUMB1/3 did not differ from the parental controls (Figure 4D-E).

Next, in order to elucidate the signaling pathways and molecular and cellular mechanisms triggered by the CD44 isoforms, we analyzed by RNAseq HCT116 and SW480 cells ectopically expressing CD44s and CD44v6. After dimension reduction with principal component analysis (PCA), the samples separated by group (i.e. CD44s-OE, CD44v6-OE, and controls) (Figure 5A). Notably, the CD44s-OE samples showed most distinct expression in both cell lines when compared to the parental and CD44v6-OE cell lines. In HCT116, the CD44v6 samples shared most similarity with the CD44s samples, while in SW480, the CD44v6 samples were most similar to the parental cell line. Thus, we observed both an isoform independent effect, presumably as the result of the ectopic CD44 expression (and most dominantly visible in HCT116), and an isoform dependent effect as depicted by the separation of CD44s and CD44v6 samples (Figure 5A). As expected, differential expression analysis of the CD44s and v6 isoforms overexpressing samples compared with the parental cell lines revealed an overall upregulation of gene expression (Figure 5-figure supplement 1 A). Next, in order to identify which genes are specifically upregulated by the different CD44 isoforms, we performed differential expression analysis between the CD44s samples and the CD44v6 samples. To this aim, we employed k-means clustering on the scaled expression values to separate genes specific for the CD44s isoform (e.g. *SPARC, ZEB1, VIM*), the CD44v6 isoform (e.g. *IL32, TACSTD2, CSF2*), and genes that were indiscriminative for the CD44v6 isoform or the

parental cell lines (e.g. *MAL2, ESRP1, CDH1*) (Figure 5B). Finally, to identify the most distinct differences in signaling pathways and GO functional categories, we performed a gene set enrichment analysis (GSEA) by comparing the CD44s- with the CD44v6-overexpressing samples in the individual cell lines. Among the significantly altered pathways (normalized enrichment score > 1, pval < 0.05), epithelial mesenchymal transition (EMT) was the only one upregulated in CD44s vs. CD44v6 in both cell lines (Figure 5C-D). Additional pathways and GO categories activated by CD44s appeared to be cell line specific, e.g. Wnt beta catenin signaling (HCT116) and oxidative phosphorylation (SW480). Of note, the detailed GSEA analysis evidenced how several inflammatory (TNF/NFκB; IL6/JAK/STAT3; IFα/γ; ILK2/STAT5) and signaling (KRAS, MYC, E2F) pathways were common to both CD44s and v6, presumably as the result of the ectopic CD44 expression, regardless of the isoform (Figure 5-figure supplement 1B).

Increased ZEB1 and decreased ESRP1 expression correlate with the NUMB2/4 and CD44s isoforms and with poor overall survival

In order to assess the clinical relevance of the results obtained with the SW480 and HCT116 cell lines, we analyzed RNAseq data from patient-derived colon cancers available from the public domain and the scientific literature. To this aim, the TCGA Splicing Variants Database (TSVdb; www.tsvdb.com) was employed to integrate clinical follow-up data with RBP and AS expression profiles obtained from The Cancer Genome Atlas project (TCGA) and from the Guinney et al study[22] on the classification of human colon cancers into four consensus molecular subtypes (CMS1–4). The main limitation of this approach is the low representation of quasi-mesenchymal (EpCAM^{lo}-like) subpopulations in bulk RNAseq preparations and the masking effect that the majority of epithelial (EpCAM^{hi}-like) cancer cells are likely to cause. To identify tumors enriched in EpCAM^{lo}-like cells, we first stratified them based on *ZEB1* expression (*ZEB1*>8.6: ZEB1^{hi}; ZEB1<8.3: ZEB1^{lo}; 8.2<ZEB1<8.6: Intermediate). Subsequently, we used *ESPR1* expression levels to further define the tumors into *ZEB1*^{hi}*ESRP1*^{lo} (*ESRP1*<11.8; hereafter referred

to as *ZEB1*^{hi}), *ZEB1*^{lo}*ESRP1*^{hi} (*ESRP1*>11.6; hereafter referred to as *ZEB1*^{lo}). Tumors with intermediate *ZEB1* expression levels and tumors with *ESRP1* expression levels outside these thresholds were defined as intermediate (Figure 6A). Kaplan-Meier analysis showed that *ZEB1*^{hi} tumors have an overall decreased survival probability (p = 0.045) (Figure 6B). Next, we compared the expression of CD44 and NUMB isoforms across the *ZEB1*$^{hi/lo}$ tumors. Notably, while no significant differences were observed based on the expression level of the whole CD44 and NUMB genes, significant differences were found for their specific isoforms (Figure 6C). Analysis of the specific isoforms expression across the different consensus molecular subtypes[22] revealed elevated CD44s and NUMB2/4 expression in the CMS4 subtype, known to be enriched in mesenchymal lineages in tumor and TME cells, and strongly associated with poor survival and the greatest propensity to form distant metastases (Figure 6D). Likewise, the majority of the *ZEB1*^{hi} group was composed of the CMS4 subtype (72%), while the *ZEB1*^{lo} group was mainly contributed by CMS2 (49%) and CMS3 tumors (31%), with few CMS4 tumors (1%) (Figure 6E).

Next, we correlated the expression of CD44s/v6 isoforms in patient-derived colon tumors with the differentially expressed genes (DEGs) identified in the isoform-overexpressing cell lines (Figure 7A). While overall *CD44* expression correlated with both isoforms, the DEGs from the CD44s-OE samples showed specific correlation with CD44s expression in patient-derived tumors (e.g. *SPARC, ZEB1*), the DEGs from the CD44v6 samples correlated with CD44v6 but not with CD44s (e.g. *KDF1, ESRP1*).

Last, we correlated the CD44 and NUMB isoforms expression in patient-derived colon cancers with functional signatures obtained by averaging the scaled expression levels for each of the hallmark sets[23]. The CD44s and NUMB2/4 isoforms showed overall similar correlating hallmarks and pathways. However, the same was not true when compared to the CD44v6- and NUMB1/3-associated functional signatures. Here, most invasion/metastasis-relevant hallmarks (e.g. EMT, angiogenesis, apical junctions) showed a positive correlation with CD44s and NUMB2/4, though not with CD44v6 and NUMB1/3 (Figure 7B).

In sum, we confirmed a switch in isoform expression (CD44v6 vs. CD44s and NUMB1/3 vs. NUMB2/4) as a function of *ESRP1* and *ZEB1* expression in colon cancer. Expression of the EpCAM^{lo}–specific isoforms (CD44s and NUMB2/4) is elevated in CMS4 tumors overall survival.

Upregulation of the NUMB2/4 and CD44s isoforms is common to quasi-mesenchymal cells from cancers other than colon.

In order to assess whether the preferential expression of the NUMB2/4 and CD44s isoforms is specific to the modalities of local invasion and distant metastasis characteristic of colon cancer, we interrogated expression profiling data previously obtained by comparing epithelial and quasi-mesenchymal subpopulations from ovarian (OV90) and cervical (SKOV6) cancer cell lines (*manuscript in preparation*). Ovarian cancer, because of the distinct anatomical localization of the primary lesion, metastasizes the abdominal cavity with very different modalities than colon cancer, namely by peritoneal dissemination rather than local dissemination into the stroma microenvironment followed by intra- and extravasation of the portal blood stream[34,35]. On the other hand, metastasis in carcinoma of the cervix occurs both by lymphatic or hematogenous spread to the lung, liver, and bones. We asked whether, notwithstanding the distinctive patterns of metastatic spread, the CD44s and NUMB2/4 isoforms were preferentially expressed in the corresponding EpCAM^{lo} RNAseq profiles. To this aim, EpCAM$^{hi/lo}$ subpopulations from OV90 and SKOV6 were sorted and analyzed by RNAseq and RTqPCR, similar to our previous study on colon cancer[17]. As shown in Figure 7-figure supplement 1, both NUMB2/4 and CD44s isoforms appear to be upregulated in the OV90 and SKOV6 cell lines, as also validated by RTqPCR.

Discussion

The capacity to invade the tumor microenvironment and to form distant metastases undoubtedly represents the most clinically relevant hallmark of epithelial cancer cells. However, the complexity and diversity of the obstacles that carcinoma cells encounter along the invasion-metastasis cascade require transient and reversible changes that cannot be explained by the *de novo* acquisition of genetic alterations. Instead, epigenetic (non-mutational) modifications underlie phenotypic plasticity, i.e. the capacity of cancer cells with a given genotype to acquire more than one phenotype in a context-dependent fashion[36]. Epithelial-to-mesenchymal and mesenchymal-to-epithelial transitions (EMT/MET) are central to the phenotypic plasticity characteristic of metastasizing carcinoma cells and are prompted by a broad spectrum of epigenetic mechanisms ranging from chromatin remodeling by histone modifications, DNA promoter methylation, non-coding RNAs, and alternative splicing (AS)[37]. Here, we have taken advantage of our previous identification of phenotypic plastic and highly metastatic EpCAM^{lo} colon cancer cells[17] to characterize the genome-wide AS events that accompany EMT/MET state transitions between the epithelial bulk (EpCAM^{hi}) and the quasi-mesenchymal subpopulation.

In view of the central role played by RNA-binding proteins in eliciting AS, we first identified RBP-coding genes differentially expressed between the EpCAM^{lo} and EpCAM^{hi} fractions of two commonly employed colon cancer cell lines , representative of the chromosomal- and microsatellite-instable subtypes (SW480, CIN; HCT116, MIN)[38]. The Epithelial Splicing Regulatory Protein 1 and 2 genes (*ESRP1/2*)[39], the "*splicing masterminds*" of EMT[40,41], were found among the top downregulated RBP-coding genes in EpCAM^{lo} colon cancer cells, as part of a self-enforcing feedback loop with the EMT-TF *ZEB1*[24]. Accordingly, *ZEB1* upregulation in EpCAM^{lo} colon cancer cells is invariably accompanied by *ESRP1/2* downregulation, and *ZEB1*^{hi}/*ESRP1*^{lo} colon cancers, predominantly belonging to the mesenchymal CMS4 subgroup, have a significantly worse survival outcome when compared with *ZEB1*^{lo}/*ESRP1*^{hi} patients.

Apart from *ESRP1*, several other RBP-coding genes were found to be differentially expressed between epithelial and quasi-mesenchymal colon cancer cells. Whereas the majority of RBP-coding DEGs, like *ESRP1*, appear to be downregulated upon EMT induction (*ESRP1*/*2*, *RBM14*/*19*/*47*, *MBNL3*, *HNRPAB*/*PF*, *USAF2*), others were activated in the quasi-mesenchymal EpCAM^{lo} fraction (*NOVA2*, *MBNL2*, *QKI*, *SRSF5*, *HNRNPH*, *RBM24*/*43*). Accordingly, in patient-derived colon cancers stratified according to their consensus molecular signature, the same *QKI*, *RBM24*, and *MBNL2* genes were found to have increased expression in CMS4 tumors, known for their pronounced mesenchymal composition and poor prognosis[22]. Of note, the mesenchymal nature of CMS4 tumors has previously been questioned as these lesions often feature pronounced infiltration from the surrounding microenvironment, the extent of which might cover their true cellular identity other than representing a mere contamination from the tumor microenvironment[42,43]. As shown in our previous study[17], the EpCAM^{lo} cells do represent *bona fide* quasi-mesenchymal colon cancer cells, enriched among CMS4 cases, and likely responsible for their poor prognosis. The observed upregulation of RBPs such as quaking (*QKI*) is caused by the presence in its 3'UTR of target sequences of the miR-200 family of microRNAs[44,45]. The latter is analogous to the regulation of the expression of the EMT-TF *ZEB1* gene, whose activation during EMT is regulated by the same microRNA family[46]. Accordingly, the significantly reduced levels of all five miR-200 members in EpCAM^{lo} cells[17] underlies the coordinated upregulation of both *ZEB1* and *QKI*.

The here observed *RBM47* downregulation in CMS4 colon cancers is in agreement with a previous report on its decreased protein expression during EMT in association with metastasis in a cohort of primary CRCs[47]. On the other hand, the increased expression of other RBP-coding genes such as *RBM24* and *MBNL2* (muscleblind-like 2) in CMS4 tumors and in EpCAM^{lo} cells is in sharp contradiction with their alleged tumor suppressing roles in colon and other cancers[48,49]. Of note, MBNL2 regulates cancer migration and invasion through PI3K/AKT-mediated EMT[49] and its overexpression in breast and cancer cell lines inhibits their metastatic potential[50]. In contrast to *MBNL2*, *MBNL3*, a distinct member of the

344 muscleblind family, is downregulated in EpCAM^{lo} colon cancer cells, similar to what reported in prostate
345 cancer by Lu and colleagues[51]. *NOVA2*, a member of the Nova family of neuron-specific RNA-binding
346 proteins, was also upregulated in the quasi-mesenchymal cells from both cell lines, possibly as the result
347 of the differential expression of miR-7-5p[52], as previously shown in non-small cell lung[52] and prostate[51]
348 cancer. The identification the AS targets downstream of specific RBPs in quasi-mesenchymal cancer cells
349 from different malignancies will likely clarify these apparent contradictions and shed light the functional
350 roles of distinct members of the splicing machinery in EMT and metastasis.

351 The spectrum of AS target genes downstream of the RBPs differentially expressed in EpCAM^{lo} colon
352 cancer cells appears extremely broad when it comes to specific cellular processes or signaling pathways.
353 Nonetheless, comparison of our RNAseq data with KD studies of specific RBPs from the public domain
354 (*ESRP1*/*2*[19], *RBM47*[18], and *QKI* [GEO Accession: GSM4677985]) allowed us to identify common and
355 unique AS target genes associated with specific downstream effectors. By following this admittedly
356 imperfect approach, the top 4 AS targets common to all of the above-mentioned RBPs notwithstanding
357 their up- or downregulation in EpCAM^{lo} colon cancer cells, i.e. *CTNND1* (δ- or p120-catenin), *LSR*
358 (Lipolysis Stimulated Lipoprotein Receptor), *SLK* (STE20 Like Kinase), and *TCF7L2* (Transcription Factor 7-
359 Like 2, or TCF4) are known regulators and effectors of epithelial-to-mesenchymal transition[27-30], thus
360 pointing to the central role played by alternative splicing in the regulation of EMT in the malignant
361 evolution of colon cancer.

362 Here, we have focused on CD44 and NUMB as two ESRP1-specific AS target genes with well-established
363 functional roles in EMT and in cancer invasion and metastasis. The CD44s and NUMB2/4 isoforms
364 appear to be specifically expressed in quasi-mesenchymal colon cancer cells both from the immortalized
365 cell lines and from patient-derived tumors, with a striking enrichment in the CMS4 subgroup of colon
366 cancer patients. In contrast, the CD44v6 and NUMB1/3 isoforms are preferentially expressed in the
367 epithelial bulk of the tumor. The latter, as far as CD44v6 is concerned, contrasts what previously

368 reported by Todaro et al.[33] where this specific isoform was found to earmark the colon cancer stem cells
369 (CSCs) which underlie metastasis. CD44v6 and other 'variable' CD44 isoforms (CD44v4-10) earmark *Lgr5*$^{+}$
370 intestinal stem cells (ISCs), i.e. the cells of origin of intestinal tumors, and accordingly promote adenoma
371 formation *in vivo*[53-55]. A plausible explanation for the discordant results lies in the epithelial nature of the
372 models employed in the above study and in the requirement of both EMT and MET for the completion
373 of the invasion-metastasis cascade[5]. By employing tumor spheres and freshly sorted CD133^{+} tumor cells,
374 Todaro et al. focused on epithelial CSCs where, as observed in normal ISCs, the CD44v6 isoform is
375 predominantly expressed, and is necessary for EMT to occur upon interaction with c-MET[33]. The CD44v6
376 isoform is required for c-MET activation by hepatocyte growth factor (HGF, or scatter factor)[56] and as
377 such plays an essential role in triggering EMT at the invasive front where tumor cells are exposed to
378 these TME-secreted factors. Our own immunoprecipitation studies confirmed that CD44v6 but not
379 CD44s binds to cMET in response to HGF stimulation (*data not shown*). Therefore, HGF/SF stimulation of
380 colon cancer cells along the invasive front will trigger the acquisition of quasi-mesenchymal
381 characteristics and the AS-driven switch from CD44v6 to CD44s, the latter unable to bind HGF and as
382 such controlling the extension of EMT activation. The reverse switch will take place upon the activation
383 of the mesenchymal-to-epithelial transitions necessary for the colonization of the distal metastatic site.
384 From this perspective, both CD44 isoforms are essential for the completion of the invasion-metastasis
385 cascade.
386 The functional relevance of the CD44s isoforms has been highlighted in malignancies other than colon
387 cancer, namely in prostate[51] and breast cancer where it activates, among others, PDGFRβ/Stat3 and Akt
388 signaling to promote EMT and CSC traits[15,57]. GO analysis of the RNAseq profiles from colon cancer cells
389 ectopically expressing CD44s highlighted a broader spectrum of signaling pathways likely to underlie
390 EMT. Accordingly, analysis of RNAseq data from primary colon cancers stratified for their CD44s
391 expression revealed an equally broad spectrum of downstream EMT-related biological processes. Of

note, among the DEGs identified upon CD44s ectopic expression which correlate with *ZEB1*^{hi}/*ESRP1*^{lo} (and CMS4) colon cancers, the *SPARC* gene, a partial EMT marker in the EpCAM$^{hi/lo}$ state transitions[17], was found.

Expression of NUMB2/4 isoforms both in cells lines and in patient-derived colon tumors is associated with signaling pathways and GO categories largely overlapping with those linked to CD44s (and CD44v6 with NUMB1/3), possibly suggesting synergism between AS at these genes. Accordingly, NUMB is involved in a broad spectrum of cellular phenotypes in homeostasis and in cancer where it mainly function as a tumor suppressor[32]. NUMB inhibits EMT by suppressing the Notch signaling pathway. As such, downregulation of NUMB can induce an EMT phenotype in isoform-specific fashion. Analysis of colon cancer cells individually overexpressing each of the four isoforms revealed an increased basal Notch signaling in NUMB2 and 4, as shown by the expression of the 'universal' targets *HES1* and *HEY1*. Instead, ectopic expression of NUMB1/3 resulted in increased transcriptional levels of the more atypical Notch signaling target *ID2*. Although the functional consequences of the NUMB2/4 (and 1/3) isoforms on Notch regulation of EMT is yet unclear, it seems plausible that the complex network of AS targets activated downstream the RBP-coding DEGs, including CD44, NUMB and many others as shown here, will eventually lead to the 'just-right' level of plasticity needed to allow both the 'mesenchymalization' during local invasion and systemic dissemination, and the reacquisition of epithelial features at the distant site of metastasis.

Overall, it appears that alternative splicing substantially contributes to the epigenetic mechanisms that underlie EMT/MET in cancer metastasis. From this perspective, several aspects of our study are novel: first, the identification of colon cancer specific AS target genes paralleled by the corresponding RNA-binding proteins which, when stratified according to the CMS classification of colon cancers, reveal notable differences and consequences on patients' survival. Moreover, the results of the functional analysis of AS at the CD44 gene contrast what previously reported[33] and shed new light on the relevance

of the standard and v6 isoforms in the migrating CSC model[5]. Comparison of the RBP/AS analysis among colon, cervical and ovarian cancer, highlights how, although the majority of AS targets are common to different types of malignancies in RBP-specific fashion, notable differences also exist possibly in reflection of the specific modalities of local dissemination and distal metastasis formation in different cancers. Also, the use of immortalized cell lines for the analysis of epithelial and quasi-mesenchymal tumor cell subpopulations represents an original approach yet based on an "old-fashioned" laboratory reagent[17]. Finally, the systematic elucidation of the RBPs and AS targets which underlie phenotypic plasticity in different types of cancer will provide novel tumor-specific targets for therapeutic intervention based on small molecule inhibitors and even RNA vaccination.

Materials and Methods

Key Resources Table				
Reagent type (species) or resource	**Designation**	**Source or reference**	**Identifiers**	**Additional information**
Cell line(Homo sapiens)	HCT116 (adult colorectal carcinoma)	ECACC	Cat# 91091005, RRID:CVCL_0291	
Cell line(Homo sapiens)	SW480 (adult colorectal carcinoma)	ECACC	Cat# 87092801, RRID:CVCL_0546	
Transfected construct (Homo sapiens)	human-ESRP1 shRNA	Horizon	Cat#V3THS_400802	Lentiviral construct to transfect and express the shRNA.
Antibody	Anti-human ZEB1 (rabbit monoclonal)	Cell Signaling	Cat# 3396, RRID:AB_1904164	WB (1:1000)
Antibody	Anti-human ESRP1 (rabbit polyclonal)	Thermo Fisher	Cat# PA5-11520, RRID:AB__2899836	WB (1:1000)
Antibody	Anti-human CD44s (mouse monoclonal)	Thermo Fisher	Cat# MA5-13890, RRID:AB_10986810	WB (1:100)
Antibody	Anti-human CD44v6 (mouse monoclonal)	Abcam	Cat#ab78960, RRID:AB_1603730	WB (1:1000)
Antibody	Anti-human NUMB (rabbit monoclonal)	Cell Signaling	Cat#2756, RRID:AB_2534177	WB (1:1000)
Antibody	Anti-human B-actin (rabbit monoclonal)	Cell Signaling	Cat#8457,RRID:AB_10950489	WB (1:2000)
Antibody	Anti-mouse CD44-APC (rat monoclonal)	BD Pharmingen	Cat# 559250, RRID:AB_398661	FACS (1 µg/10^6 cells)
Antibody	Anti-human EpCAM-FITC (mouse monoclonal)	GeneTex	Cat# GTX30708, RRID:AB_1240769	FACS (1 µg/10^6 cells)
recombinant DNA reagent	ESRP1 cDNA ORF Clone (human)	Sino Biological	Cat# HG13708-UT	
recombinant DNA reagent	pcDNA empty vector (plasmid)	Gift from Ron Smits		
recombinant DNA reagent	pcDNA-human-CD44s (plasmid)	Gift from Véronique Orian-Rousseau		
recombinant DNA reagent	pUC57-human-CD44v6 (plasmid)	Gift from Véronique		

		Orian-Rousseau		
recombinant DNA reagent	pcDNA-human-NUMB1 (plasmid)	Gift from Salvatore Pece		
recombinant DNA reagent	pcDNA-human-NUMB2 (plasmid)	Gift from Salvatore Pece		
recombinant DNA reagent	pcDNA-human-NUMB3 (plasmid)	Gift from Salvatore Pece		
recombinant DNA reagent	pcDNA-human-NUMB4 (plasmid)	Gift from Salvatore Pece		
recombinant DNA reagent	shZEB1	Andrea Sacchetti et al., 2021	Cat# 1864	
recombinant DNA reagent	pSLIK-Hygro	Addgene	Cat# 25737	
software, algorithm	R	Seurat, GSVA, MAGIC (Stuart et al., 2019; van Dijk et al., 2018; Hanzelmann et al., 2013)	RRID:SCR_007322, RRID:SCR_021058	Version 4.0.4
software, algorithm	Python	Velocyto, scVelo (La Manno et al., 2018 ; Bergen et al., 2020)	RRID:SCR_018167, RRID:SCR_018168	Version 3.8.3
software, algorithm	STAR	Dobin, A. et al. 2013.	RRID:SCR_004463	
software, algorithm	MISO	Katz, Yet al., .2010.	RRID:SCR_003124	

Cell Cultures

The human colon cancer cell lines HCT116 and SW480, obtained from the European Collection of Authenticated Cell Culture (ECACC), were cultured in DMEM (11965092, Thermo Fisher Scientific) with 10% FBS (Thermo Fisher Scientific), 1% penicillin/streptomycin (Thermo Fisher Scientific, 15140122), and 1% glutamine (Gibco, 25030024), in humidified atmosphere at 37°C with 5% CO_2. Both cell lines tested negative for mycoplasma. The identity of each cell line was confirmed by DNA fingerprinting (STR) with microsatellite markers (Amelogenin, CSF1PO, D13S317, D16S539, D5S818, D7S820, THO1, TPOX, vWA, D8S1179, FGA, Penta E, Penta D, D18S51, D3S1358, D21S11) and compared with the analogous data provided by ATCC, EACC, and https://web.expasy.org/cellosaurus/ (data not shown).

Plasmid transfection and lentiviral transduction

Stable transfection of the *ESRP1* (Sino Biological plasmid # HG13708-UT), *CD44s*, *CD44v6*, and NUMB1-4 (from V.O.R.) expression plasmids was performed using FuGENE HD transfection reagent (Promega, E2311) according to the manufacturer's protocol and selected with Geneticin (Gibco, 10131035). As for the knockdown constructs, the *ESRP1*-shRNA plasmid (Horizon, V3THS_335722) was packaged by pPAX2 (Addgene # 12260) and pMD2.G (Addgene # 12259) into HEK293T. The virus-containing supernatant was collected 24 hrs. after transfection, filtered, and employed to infect the HCT116 and SW480 cell line. Selection was applied with 750 ng/ml puromycin (Invivogen, San Diego, USA) or 800 μg/ml of Geneticin selection for 1-2 weeks. The efficiency of overexpression and knockdown was assessed by qPCR and western blot 48-72 h after transfection.

qRT-PCR and PCR analyses

Total RNA was isolated using TRIzol reagent (Thermo Fisher Scientific, 15596018) and was reverse-transcribed using high-capacity cDNA reverse transcription kit (Life Technologies, 4368814), according to the manufacturer's instructions. qRT-PCR was performed using the Fast SYBR Green Master Mix (Thermo Fisher Scientific) on an Applied Biosystems StepOne Plus Real-Time Thermal Cycling Research with three replicates per group. Relative gene expression was determined by normalizing the expression of each target gene to GAPDH. Results were analyzed using the 2-(ΔΔCt) method. To validate isoform switches by RT-PCR, CD44-specific primers were as listed in Supplementary File 3.

Western analysis

Cells were lysed in 2X Laemmli buffer containing 4% SDS, 48% Tris 0.5M pH6.8, 20% glycerol, 18% H_2O, bromophenol blue and 10% 1M DTT, and subjected to sodium dodecyl sulfate (SDS)- polyacrylamide gel electrophoresis (PAGE), followed by transfer onto polyvinylidene fluoride (PVDF) membranes (Bio-Rad). After blocking with 5% milk in TBS-Tween, the membranes were incubated with primary antibodies

against ZEB1 (1:1000, Cell Signaling, #3396), ESRP1 (1:1000, Invitrogen, PA5-11520), CD44s (1:100, Invitrogen, MA5-13890), CD44v6 (1:1000, Abcam, VFF-7), NUMB (1:1000, Cell Signaling, C29G11) and β-actin (1:2000, Cell Signaling, 8547), followed by polyclonal goat anti-mouse/ rabbit immunoglobulins horseradish peroxidase (HRP)-conjugated secondary antibody (Dako) at appropriate dilutions. The signals were detected with Pierce ECT western blotting subtrade (Thermo) using Amersham AI600 (GE Healthcare, USA).

Flow cytometry analysis and sorting

Single-cell suspensions generated in PBS supplemented with 1% FBS were incubated with anti-EpCAM-FITC (1:20, Genetex, GTX30708), and anti-CD44-APC (1:20, BD Pharmingen, 559250) antibodies for 30 min on ice and analyzed on a FACSAria III Cell Sorter (BD Biosciences). $CD44^{hi}EpCAM^{hi}$and $CD44^{hi}EpCAM^{lo}$ HCT116 and SW480 cells were sorted and cultured in humidified atmosphere at 37°C with 5% CO_2 for 3-5 days before collecting RNA or protein, as previously described[17]. The subpopulation of cells mapping in between the $CD44^{hi}EpCAM^{hi}$ and $CD44^{hi}EpCAM^{lo}$ gates was labeled as intermediate and was further not employed for analysis.

MTT assay

For MTT assay, 2×10^3 HCT116, SW480 parental, CD44v6, CD44s, and NUMB1-4 OE cells were plated in 96 well plates and incubated at 37°C, 5% CO_2. 24 hours later, in the culture medium was supplemented with 100µl 0.45 mg/mL MTT (3-(4,5-dimethylthiazol-2-yl)-2,5-diphenyltetrazolium bromide; Sigma-Aldrich) and again incubated for 3 hrs.. The 96-well plates were then centrifuged at 1,000 rpm for 5 min and the culture medium removed. MTT formazan precipitates were solubilized with DMSO. OD reading was performed at 595 nm with microplate reader (Model 550, Bio-Rad). Background measurements were subtracted from each data point. Experiments were performed in duplicate for each individual cell line and drug. Cell numbers were calculated every 24 hrs. for a 6 days period for proliferation analysis.

Cell migration assay

Migration assay were conducted with 8-µm pore PET transwell inserts (BD Falcon™) and TC-treated multi-well cell culture plate (BD Falcon™). 5×10^4 cells were seeded in 100 µl of serum-free growth medium in the top chamber. Growth medium containing 10% FBS was used as a chemoattractant in the lower chamber. After 24 hrs., cells migrated to the lower chamber were fixed with 4% PFA, stained with 0.1% trypan blue solution, and counted under the microscope.

Mouse spleen transplantation

All mice experiment were implemented according to the Code of Practice for Animal Experiment in Cancer Research from the Netherlands Inspectorate for Health Protections, Commodities and Veterinary Public Health. Mice were fed in the Erasmus MC animal facility (EDC). NOD.Cg-Prkdc^{scid} Il2rg^{tm1Wjl}/SzJ (NSG) mice from 8 to12 week-old were used for spleen transplantation. Anesthetics Ketamine (Ketalin®, 0.12 mg/ml) and xylazine (Rompun®, 0.61mg/ml) were given intraperitoneally, while the analgesic Carpofen (Rimadyl®, 5 mg/ml) was injected subcutaneously. $5x10^4$ HCT116 and SW480 cells resuspended in 50 µl PBS were injected into the exposed spleen with an insulin syringe and left for 15 minutes before splenectomy. Transplanted mice were sacrificed after 4 and 8 weeks and analyzed for the presence of liver metastases.

Alternative splicing analysis

The following public available RNASeq (SRA database) data relative to RBP (RNA binding protein) knock-down (KD) studies were used: ESRP1-KD and RMB47-KD in the human non-small cell lung cancer cell line H358[18] with accession ID SRP066789 and SRP066793; ESRP2-KD in the human prostate adenocarcinoma cancer cell line LNCaP[19] with accession ID SRP191570; the QKI-KD in the oral squamous cell carcinoma cell line CAL27 datasets with accession number SRX8772405. Together with our own EpCAM$^{hi/lo}$ RNASeq data obtained from the colon cancer cell lines[17], the sequencing reads were mapped

to GRCh37.p13.genome by STAR[20] (https://www.gencodegenes.org/human/release_19.html). MISO[21] was used to quantify AS events with annotation from https://miso.readthedocs.io/en/fastmiso/index.html#iso-centric. The MISO uses the alternative exon reads and adjacent conservative reads to measure the percentage of transcript isoform with specific exon included, termed Percentage Spliced In (PSI or Ψ). The PSI ranges from 0 (i.e. no isoform includes a specific alternative exon) to 1 (i.e. all of the isoforms detected comprise the alternative exon).

We removed alternative events with low expression of related transcript isoforms if less than 3 samples in a dataset had more than 10 informative reads to calculate the PSI. Next, we compared the PSI between RBPs KD and wild type in each cell line, as well as the PSI between $EpCAM^{hi}$ and $EpCAM^{lo}$ groups in the SW480 and HCT116 colon cancer cell lines. AS events were defined as differentially spliced events when the difference of mean PSI between two groups (Δpsi; differential Percentage Spliced In) was >10%.

RNAseq analysis

RNA quality was first evaluated by NanoDrop and further purified by DNAse treatment followed by the TURBO DNA-free Kit protocol (Invitrogen). Samples were sequenced with the DNA nanoball (DNB) seq protocol (BGI) to a depth of 50 million reads per sample. Adapter sequences and low-quality sequences were filtered from the data using SOAPnuke software (BGI). Reads were aligned to the human reference genome build hg19 with the RNAseq aligner STAR (v2.7.9a) and the Homo sapiens GENCODE v35 annotation. Duplicates were marked with Sambamba (0.8.0) and raw counts were summed using FeatureCounts (subread 2.0.3). Downstream analysis was performed in R using the DESeq2 package (v1.30.1). After variance stabilizing transformation, principal component analysis was performed on each cell line separately. Differentially expressed genes were identified by comparing the different groups of ectopically expressing CD44 samples with a Wald test, and by selecting the genes with

absolute log fold change above 1.5 and padj < 0.1. Gene set enrichment analysis was performed with the Fsgsea package using the HallMark geneset from the molecular signature database, and by selecting significant pathways based on normalized enrichment score (NES) > 1 and pvalue < 0.05.

RNAseq data from primary (patient-derived) colon cancers

Patient data from The Cancer Genome Atlas (TCGA), with annotation of the consensus molecular subtypes (CMS) as described in Guinney et al.[22] were integrated with splicing data from the TCGA splicing variant database (TSVdb, www.tsvdb.com). For splicing analysis, RNA-seq by expectation maximization (RSEM) values were log transformed and expression levels of each isoform (CD44std: isoform_uc001mvx, CD44v6: exon_chr11.35226059.35226187, NUMB1: isoform_uc001xny, NUMB2: isoform_uc001xoa, NUMB3: isoform_uc001xnz, NUMB4: isoform_uc001xob) were annotated to the patients. Isoform expression was compared in groups based on the CMS groups and tumor expression levels (*ZEB1*, *ESRP1*). Tumors were stratified on *ZEB1* expression levels using a log rank test top optimize overall survival differences (thresholds: 8.3, 8.6). Next, ESRP1 expression was used to purify the groups into $ZEB1^{hi}ESRP1^{lo}$ and $ZEB1^{lo}ESRP1^{hi}$ (thresholds: 11.6, 11.8). Survival analysis was done using the Kaplan-Meier method with the survival and survminer packages in R. Correlation analysis was done by computing the Pearson Correlation between the isoforms and whole gene expression levels as processed in Guinney et al.[22]. Likewise, association between isoform expression and pathway activity was evaluated by computing the Pearson Correlation between the isoforms and the average scaled expression values of the pathways, as defined in the HallMark gene set from the molecular signature database[23].

Data accessibility

The RNA-sequencing data from this study have been submitted to the Gene Expression Omnibus (GEO) database under the accession number GSE192877. Other data referenced in this study are publicly

554 available and can be accessed from the GEO using GSE154927[17] , GSE154730 and Synapse using

555 identifier syn2623706[22] .

556

557

558 **Acknowledgements**

559 We are grateful to Dr. Juan Valcarcel, (CRG, Barcelona, Spain), for his critical reading of the manuscript.

560

Figure Legends

Figure 1. *ZEB1* and *ESRP1* differential expression in quasi-mesenchymal and highly metastatic EpCAM^{lo} colon cancer cells.

A. Gene rank plot showing differentially expressed genes between EpCAM^{hi} and EpCAM^{lo} with combined analysis of HCT116 and SW480.

B. RT-qPCR *ESRP1*- and *ZEB1* expression analysis of HCT116 and SW480 EpCAM^{hi}, EpCAM^{lo}, and bulk subpopulations. *GAPDH* expression was used as control (Means±SEM, n=3). ** = $p<0.01$.

C. ESRP1 and ZEB1 western analysis in HCT116 and SW480 EpCAM^{hi}, EpCAM^{lo}, and bulk fractions. β-actin was used as loading control.

D. RT-qPCR and western analysis of *ZEB1* and *ESRP1* expression in *ZEB1*-OE and -KD HCT116 and SW480 cells. Expression values were normalized in each sample with those from the parental HCT116 and SW480 cell lines. HCT116 and SW480 cells transduced with the sh*ZEB1* lentivirus were induced by 1 µg/mL doxycycline for 72 hrs.. Expression values were normalized with those from non-induced cells; *GAPDH* expression was employed as control (Means±SEM, n=3). * = $p<0.05$, ** = $p<0.01$. β-actin was used as loading control.

E. RT-qPCR *ZEB1* and *ESRP1* expression analysis in *ESRP1*-OE and -KD HCT116 and SW480 cells. Two independent *ESRP1*-OE clones were selected for each cell line. Expression values were normalized in each sample with those from the parental HCT116 and SW480 cell lines. HCT116 and SW480 cells transduced with the sh*ESRP1* lentivirus were induced by 1 µg/mL doxycycline for 72 hrs. Two independent clones were selected for each cell line. Expression values were normalized with those from non-induced cells; *GAPDH* expression was employed as control (Means±SEM, n=3). * = $p<0.05$, ** = $p<0.01$.

F. CD44/EpCAM FACS analysis of HCT116 and SW480 EpCAM^{lo} and EpCAM^{hi} subpopulations in ESRP1-OE cells. Two independent clones are showed for each cell lines.

Figure 2. *ESRP1* downregulation in EpCAM^{lo} colon cancer cells affects alternative splicing of *CD44* and *NUMB* among a broad spectrum of downstream target genes.

A. Heatmap of common AS events between RNAseq data from a previous *ESRP1*-KD study in human non-small cell lung cancer cells (H358)[18] and our own HCT116 and SW480 EpCAM^{hi} and EpCAM^{lo} RNAseq data[17]. The gene list on the right of the heatmap encompasses AS variants earmarked by ΔPSI > 0.1.

B. *CD44* and *NUMB* exon peak plots relative to the AS analysis of the RNAseq data obtained from a previous *ESRP1*-KD study in human non-small cell lung cancer cells (H358; upper graph)[18] and from our own HCT116 (middle graph) and SW480 (lower graph) EpCAM$^{hi/lo}$ analysis[17]. Each peak plot depicts the expression of specific exons; the height of each peak is indicative of the expression level of the specific exons. CD44v: CD44 exons v2 to v10. CD44v and CD44s, and NUMB exon 12 is highlighted by gray rectangles.

C. RT-qPCR expression analysis of *CD44*s, *CD44*v6*, NUMB1/3* and *NUMB2/4* isoforms in HCT116 and SW480 EpCAM^{hi}, EpCAM^{lo}, and bulk subpopulations. Expression of the constitutive *CD44* and *NUMB* exons was employed to normalize the results (Means±SEM, n=3). ** = p<0.01.

D. Western analysis of CD44s, CD44v6 and NUMB isoforms in HCT116 and SW480 EpCAM^{hi}, EpCAM^{lo}, and bulk subpopulations. Please note that the molecular weight of CD44v6 is expected to range between 80 to 150 kDa[58,59]. β-actin was used as loading control.

Figure 3. *ESRP1* differential expression regulates *CD44* and *NUMB* AS isoforms expression.

A. RT-qPCR (left histogram panels) and western (right panel) analysis of CD44 and NUMB isoforms expression in *ESRP1*-KD (sh*ESRP1* transduced) HCT116 cells. Two independent HCT116 *ESRP1*-KD clones

were employed. Cells were induced with 1 μg/mL doxycycline for 72 hrs. before analysis. Expression of the constitutive *CD44* and *NUMB* exons was employed to normalize the results (Means±SEM, n=3). ** = p<0.01. The ratio of NUMB1/3 and NUMB2/4 bands was quantified by ImageJ and shown in bar plot. Please note that the molecular weight of CD44v6 is expected to range between 80 to 150 kDa[58,59]. β-actin was used as loading control for western blots.

B. RT-qPCR (left histogram panels) and western (right panel) analysis of CD44 and NUMB isoforms expression in *ESRP1*-KD (sh*ESRP1* transduced) SW480 cells. Two independent SW480 *ESRP1*-KD clones were employed. Cells were induced with 1 μg/mL doxycycline for 72 hrs. before analysis. Expression of the constitutive *CD44* and *NUMB* exons was employed to normalize the results (Means±SEM, n=3). ** = p<0.01. The ratio of NUMB1/3 and NUMB2/4 bands was quantified by ImageJ and shown in bar plot. Please note that the molecular weight of CD44v6 is expected to range between 80 to 150 kDa[58,59]. β-actin was used as loading control for western blots.

C. RT-qPCR (left histogram panels) and western (right panel) analysis of CD44 and NUMB isoforms expression in *ESRP1*-OE HCT116 cells. Two independent HCT116 *ESRP1*-OE clones were employed. . Expression of the constitutive *CD44* and *NUMB* exons was employed to normalize the results (Means±SEM, n=3). ** = p<0.01. The ratio of NUMB1/3 and NUMB2/4 bands was quantified by ImageJ and shown in bar plot. Please note that the molecular weight of CD44v6 is expected to range between 80 to 150 kDa[58,59]. β-actin was used as loading control for western blots.

D. RT-qPCR (left histogram panels) and western (right panel) analysis of CD44 and NUMB isoforms expression in *ESRP1*-OE SW480 cells. Expression of the constitutive *CD44* and *NUMB* exons was employed to normalize the results (Means±SEM, n=3). ** = p<0.01. The ratio of NUMB1/3 and NUMB2/4 bands was quantified by ImageJ and shown in bar plot. Please note that the molecular weight of CD44v6 is expected to range between 80 to 150 kDa[58,59]. β-actin was used as loading control for western blots.

Figure 4. *CD44* and *NUMB* AS isoforms have opposite functions in quasi-mesenchymal and epithelial colon cancer cells and their capacity to metastasize the liver.

A. CD44/EpCAM FACS analysis of $EpCAM^{lo}$ and $EpCAM^{hi}$ subpopulations in CD44s-OE (left) and CD44v6-OE HCT116 and SW480 cell lines. The bar charts on the right depict the percentages of $EpCAM^{lo}$ and $EpCAM^{hi}$ cells. The subpopulation of cells mapping in between, but yet outside, the $CD44^{hi}EpCAM^{hi}$ and $CD44^{hi}EpCAM^{lo}$ gates, is here labelled as 'intermediate'.

B. and **C.** CD44/EpCAM FACS analysis of $EpCAM^{lo}$ and $EpCAM^{hi}$ subpopulations in NUMB1 to 4-OE HCT116 and SW480 cells. The bar charts on the right depict the percentages of $EpCAM^{lo}$ and $EpCAM^{hi}$ cells.

D. Macroscopic images of livers from mice spleen-injected with CD44s-, CD44v6-, NUMB2/4-, and NUMB1/3-OE HCT116 cells. HCT116 $EpCAM^{lo}$ and bulk cells were used as positive control. Scale bar: 5 mm. **E.** Liver metastasis multiplicity after intrasplenic injection of CD44s-, CD44v6-, NUMB2/4-, and NUMB1/3-OE HCT116 cells. For each transplantation experiment, 5×10^4 cells were injected in the spleen of recipient NSG mouse. Six weeks after injection, mice were sacrificed and individual tumors counted. * = $p<0.05$; ** = $p<0.01$.

Figure 5. RNAseq analysis of CD44s- and CD44v6-expressing colon cancer cells reveals a broad spectrum of downstream AS targets and biological functions.

A. Principal Component Analysis (PCA) of RNAseq profiles from CD44s- and CD44v6-OE HCT116 and SW480 cell lines.

B. Heatmap of differentially expressed gene among HCT116 and SW480 CD44s-OE, CD44v6-OE, and parental cells.

C. Gene Set Enrichment Analysis (GSEA) of epithelial mesenchymal transition (EMT) in expression profiles from HCT116 and SW480 parental, CD44s-OE, and CD44v6-OE cells. Normalized enrichment score (NES) > 1, and pval < 0.05.

D. Gene Set Enrichment Analysis (GSEA) of HCT116 and SW480 expression profiles in parental, CD44s-OE, CD44v6-OE cells compared with each other. Plots show only significantly altered pathways, with normalized enrichment score (NES) > 1, and pval < 0.05.

Figure 6. Increased *ZEB1* and decreased *ESRP1* expression correlate with the NUMB2/4 and CD44s isoforms and with poor overall survival.

A. RNAseq data from the Cancer Genome Atlas (TCGA) were subdivided in 3 groups based on *ZEB1* and *ESRP1* expression level: $ZEB1^{hi}ESRP1^{lo}$ ($ZEB1^{hi}$, red dots), $ZEB1^{lo}ESRP1^{hi}$ ($ZEB1^{lo}$, blue dots), and intermediate (grey dots).

B. Kaplan Meier analysis of overall survival in the $ZEB1^{hi}ESRP1^{hi}$ and $ZEB1^{lo}ESRP1^{lo}$ patient groups.

C. Box plots showing CD44 and NUMB gene and isoforms expression across the $ZEB1^{hi}ESRP1^{lo}$, $ZEB1^{lo}ESRP1^{hi}$, and intermediate patient groups.

D. Dot plot analysis of the z-score scaled expression values of CD44s, CD44v6, NUMB1-4 isoforms across the 4 colon cancer consensus molecular subtypes (CMS).

E. Stacked bar plot showing the composition of the CMS subtypes across the $ZEB1^{hi/lo}$ and intermediate patient groups.

Figure 7. Gene and pathway correlation analyses of CD44 and NUMB isoforms in patient-derived colon cancers.

A. Gene correlation analysis showing the correlation of gene expression with CD44s and CD44v6 isoform expression in the TCGA patient cohort. Differentially expressed genes from CD44s- (red) and CD44v6-OE (blue) RNAseq data are highlighted.

B. Pathway correlation analysis showing the correlation of pathway activity CD44 and NUMB isoform expression in the TCGA patient cohort.

Supplementary Figure Legends

Figure 1-figure supplement 1. *ESRP1* and RBPs functional and expression analysis in cell lines and patient-derived colon cancers.

A. FACS isotype and compensation controls in the analysis of the HCT116 and SW480 cell lines. The gates relative to the EpCAM$^{hi/lo}$ subpopulations are specifically designed for the HCT116 and SW480 cell lines, as shown for the full staining. For the sake of simplicity and readability, the quadrants showing negative, single positive, and double positive regions, have not been repeated in the figures encompassing FACS analyses.

B. CD44/EpCAM FACS analysis of EpCAM^{lo} and EpCAM^{hi} subpopulations in ESRP1-KD (*shESRP1*-transduced) HCT116 and SW480 cells. Cells were induced with 1 μg/mL doxycycline for 72 hrs. before analysis.

C. List of RBPs differentially expressed between EpCAM^{lo} and EpCAM^{hi} subpopulation in SW480 and HCT116. The RBPs list was from reference (10).

D. Dot plot analysis of the z-score scaled RBPs' expression values across the 4 colon cancer consensus molecular subtypes (CMS; annotated according to Guinney et al.[22]. RNAseq data were obtained from the COAD (COlon-ADenoma) tumors of The Cancer Genome Atlas (TCGA) deposited in the TCGA Splicing Variants Database (TSVdb), (n=206 primary tumors).

Figure 2-figure supplement 1. *ESRP1/2-*, *RBM47-*, and *QKI*-regulated AS targets.

A. Heatmap of the alternative splicing events observed by comparing previously published RNAseq data from RBP-KD studies (ESRP1-KD in H358[18], ESRP2-KD in LNCaP[19], RBM47-KD in H358[18], and QKI-KD in CAL27 [GEO Accession: GSM4677985]) with our own HCT116/SW480 EpCAM$^{hi/lo}$ RNAseq data[17]. Shared AS targets between RBPs KD cells, and HCT116/SW480 EpCAM$^{hi/lo}$ subpopulations are shown. The gene list on the right side of the heatmap encompasses variants earmarked by ΔPSI > 0.1. The colored bars on

the left of the heatmap shows if there are variants spliced by different RPBs. Color in white means AS is not involved in.

B. PSI value of NUMB exon12 between ESRP1 KD, ESRP2 KD, RBM47 KD, QKI KD and control cells.

Figure 3-figure supplement 1. *ESRP1*, *CD44*, and *NUMB* isoforms analysis in over-expressing and knock-down colon cancer cell lines.

RT-PCR analysis of CD44 and NUMB isoforms expression in HCT116 (**A**) and SW480 (**B**) ESRP1-KD (*shESRP1*-transduced) cells, and in HCT116 (**C**) and SW480 (**D**) *ESRP1*-OE cells. Cells were induced with 1 μg/mL doxycycline for 72 hrs. before RNA isolation. *GAPDH* was used as control.

E. RT-qPCR analysis of CD44s and CD44v6 expression in HCT116 and SW480 CD44s- (left), and CD44v6-OE (right) cells. Expression of the constitutive *CD44* exons was employed to normalize the results (Means±SEM, n=3). ** = $p<0.01$.

F. Western analysis of CD44, ESRP1 and ZEB1 expression in HCT116 and SW480 CD44s- (left), and CD44v6-OE (right) cells. Please note that the molecular weight of CD44v6 is expected to range between 80 to 150 kDa[58,59]. β-actin was used as loading control for western blots.

G. RT-PCR analysis of NUMB1-4 isoforms expression in HCT116 and SW480 NUMB1-4 OE cells. Expression of the constitutive *NUMB* exons was employed to normalize the results (Means±SEM, n=3). ** = $p<0.01$.

H. Western analysis of NUMB1-4 isoforms, ESRP1, and ZEB1 expression in HCT116 and SW480 NUMB1-4 OE cells (upper panels). The ratio of NUMB1/3 and NUMB2/4 bands was quantified by ImageJ and shown in bar plot (lower histogram panels). β-actin was used as loading control for western blots.

Figure 3-figure supplement 2. *CD44* and *NUMB* isoform-specific expression affects cell migration and Notch signaling activation.

A. Migration assay analysis of HCT116 CD44s-, CD44v6-, and NUMB1/4-OE cells. EpCAM^{lo} and EpCAM^{hi} cells were used as controls. Each bar represents the mean ± SD of cells migrated to the bottom of the transwell from two independent experiments.

B. Migration assay analysis of SW480 CD44s-, CD44v6-, and NUMB1/4-OE cells. EpCAM^{lo} and EpCAM^{hi} cells were used as controls. Each bar represents the mean ± SD of cells migrated to the bottom of the transwell from two independent experiments.

C. RT-qPCR analysis of EMT-TFs in HCT116 and SW480 CD44s-, CD44v6-, and NUMB1/4-OE cells. *GAPDH* expression was used as control, normalized with the HCT116 or SW480 parental in each sample (Means±SEM, n=3). Increased gene expression is depicted by red bars, whereas downregulation – when compared with parental cells- is shown by blue bar.

D. RT-qPCR analysis of the Notch signaling pathway markers *HES1*, *HEY1*, and *ID2* in HCT116 and SW480 NUMB1/4-OE cells. *GAPDH* expression was used as control (Means±SEM, n=3). * = $p<0.05$; ** = $p<0.01$.

Figure 4-figure supplement 1. CD44 and NUMB isoforms regulate colon cancer cell proliferation.

A. Proliferation assays of HCT116 CD44s- and CD44v6-OE cells. Both OD values and cell multiplicities are shown from day 1 to 6 (Means±SEM, n=3). * = $p<0.05$; ** = $p<0.01$.

B. Proliferation assays of SW480 CD44s- and CD44v6-OE cells. Both OD values and cell multiplicities are shown from day 1 to 6 (Means±SEM, n=3). * = $p<0.05$; ** = $p<0.01$.

C. Proliferation assays of HCT116 NUMB1/4-OE cells. Both OD values and cell multiplicities are shown from day 1 to 6 (Means±SEM, n=3). ** = $p<0.01$.

D. Proliferation assays of SW480 NUMB1/4-OE cells. Both OD values and cell multiplicities are shown from day 1 to 6 (Means±SEM, n=3). ** = $p<0.01$.

Figure 5-figure supplement 1. Gene Enrichment and Pathway Analysis of CD44s- and CD44v6-overexpressing colon cancer cells.

A. Vulcano plots showing differentially expressed genes (absLFC > 2, pval < 0.01, red) by comparing parental cell lines to the CD44s- and CD44v6-OE samples in both cell lines.

B. Gene Set Enrichment Analysis of parental, CD44s- and CD44v6-OE cells compared with each other in HCT116 and SW480 cells shown in heatmap, respectively. Only significantly altered pathways (NES > 1, and pval < 0.05) are shown.

Figure 6-figure supplement 1. *CD44* and *NUMB* isoforms expression in EpCAM$^{hi/lo}$ ovarian and cervical cancer cells.

A. *CD44* and *NUMB* exon chromosome sites information from AS analysis in the ovarian and cervical cancer cell lines OV90 and SKOV6. Exon peak plot depicts the expression of different exons in the three groups; peak height is indicative of the expression level of specific exons. CD44v: CD44 exons v2 to v10. CD44v and CD44s, and NUMB exon 12 are highlighted by gray rectangles.

B. RT-qPCR expression analysis of *ESRP1*, *CD44s*, *CD44v6*, *NUMB1*/*3*, and *NUMB2*/*4* isoforms in EpCAM^{hi}, EpCAM^{lo}, and bulk subpopulations in OV90 and SKOV6 ovarian cancer cell lines. *GAPDH* expression was used as control (Means±SEM, n=3). ** = p<0.01.

Supplementary Table Legends

Supplementary File 1. List of alternative splicing targets in ESRP1 knocking down H358 line (a), HCT116 (b) and SW480 (c) EpCAM^{lo} and EpCAM^{hi} subpopulation, filtered by ΔPSI > 0.1

Supplementary File 2. List of alternative splicing targets in *ESRP1*-KD in the H358 cell line, *ESRP2*-KD in LNCaP, *RBM*47-KD in H358 line, QKI-KD in CAL27, and HCT116 and SW480 EpCAM^{lo} and EpCAM^{hi} subpopulation, filtered by ΔPSI > 0.1.

Supplementary File 3. Lists of primer sequences used for RT-PCR analysis.

Supplementary File 4. Differential expressed gene lists from the RNAseq analysis HCT116 CD44s- and CD44v6-OE cells.

Supplementary File 5. Differential expressed gene lists from the RNAseq analysis SW480 CD44s- and CD44v6-OE cells.

Supplementary File 6. List of Gene Set Enrichment Analysis (GSEA) in CD44s OE vs. CD44v6 OE vs. parental HCT116 and SW480 cells.

Supplementary File 7. List of Gene Set Variation Analysis (GSVA) in CD44s OE vs. CD44v6 OE vs. parental HCT116 and SW480 cells

Source Data Legends

Figure 1-source data-1: Original files and labelled bands of western blots in Figure 1 C-D.

Figure 2-source data-1: Original files and labelled bands of western blots in Figure 2 D.

Figure 3-source data-1: Original files and labelled bands of western blots in Figure 3 A.

Figure 3-source data-2: Original files and labelled bands of western blots in Figure 3 B.

Figure 3-source data-3: Original files and labelled bands of western blots in Figure 3 C.

Figure 3-source data-4: Original files and labelled bands of western blots in Figure 3 D.

Figure 3-figure supplement 1 -source data-1: Original files and labelled bands of PCR gels in Figure 3-figure supplement 1 A.

Figure 3-figure supplement 1 -source data-2: Original files and labelled bands of PCR gels in Figure 3-figure supplement 1 B.

Figure 3-figure supplement 1 -source data-3: Original files and labelled bands of PCR gels in Figure 3-figure supplement 1 C.

Figure 3-figure supplement 1 -source data-4: : Original files and labelled bands of PCR gels in Figure 3-figure supplement 1 D.

Figure 3-figure supplement 1 -source data-5: Original files and labelled bands of western blots in Figure 3-figure supplement 1 F.

Figure 3-figure supplement 1 -source data-6: Original files and labelled bands of western blots in Figure 3-figure supplement 1 H.

References

1 Hanahan, D. Hallmarks of Cancer: New Dimensions. *Cancer Discov* **12**, 31-46, doi:12/1/31 [pii] 10.1158/2159-8290.CD-21-1059 (2022).

2 Bernards, R. & Weinberg, R. A. A progression puzzle. *Nature* **418**, 823, doi:10.1038/418823a (2002).

3 Reiter, J. G. *et al.* Minimal functional driver gene heterogeneity among untreated metastases. *Science* **361**, 1033-1037, doi:10.1126/science.aat7171 (2018).

4 Thiery, J. P., Acloque, H., Huang, R. Y. & Nieto, M. A. Epithelial-mesenchymal transitions in development and disease. *Cell* **139**, 871-890, doi:10.1016/j.cell.2009.11.007 (2009).

5 Brabletz, T., Jung, A., Spaderna, S., Hlubek, F. & Kirchner, T. Opinion: migrating cancer stem cells - an integrated concept of malignant tumour progression. *Nat Rev Cancer* **5**, 744-749, doi:10.1038/nrc1694 (2005).

6 Fodde, R. & Brabletz, T. Wnt/beta-catenin signaling in cancer stemness and malignant behavior. *Curr Opin Cell Biol* **19**, 150-158, doi:10.1016/j.ceb.2007.02.007 (2007).

7 Teeuwssen, M. & Fodde, R. Cell Heterogeneity and Phenotypic Plasticity in Metastasis Formation: The Case of Colon Cancer. *Cancers (Basel)* **11**, doi:10.3390/cancers11091368 (2019).

8 Wang, E. T. *et al.* Alternative isoform regulation in human tissue transcriptomes. *Nature* **456**, 470-476, doi:10.1038/nature07509 (2008).

9 Blencowe, B. J. Alternative splicing: new insights from global analyses. *Cell* **126**, 37-47, doi:10.1016/j.cell.2006.06.023 (2006).

10 Fu, X. D. & Ares, M., Jr. Context-dependent control of alternative splicing by RNA-binding proteins. *Nature reviews. Genetics* **15**, 689-701, doi:10.1038/nrg3778 (2014).

11 Kahles, A. *et al.* Comprehensive Analysis of Alternative Splicing Across Tumors from 8,705 Patients. *Cancer Cell* **34**, 211-224 e216, doi:10.1016/j.ccell.2018.07.001 (2018).

12 Roy Burman, D., Das, S., Das, C. & Bhattacharya, R. Alternative splicing modulates cancer aggressiveness: role in EMT/metastasis and chemoresistance. *Mol Biol Rep* **48**, 897-914, doi:10.1007/s11033-020-06094-y (2021).

13 Oltean, S. & Bates, D. O. Hallmarks of alternative splicing in cancer. *Oncogene* **33**, 5311-5318, doi:10.1038/onc.2013.533 (2014).

14 Biamonti, G., Infantino, L., Gaglio, D. & Amato, A. An Intricate Connection between Alternative Splicing and Phenotypic Plasticity in Development and Cancer. *Cells* **9**, doi:10.3390/cells9010034 (2019).

15 Brown, R. L. *et al.* CD44 splice isoform switching in human and mouse epithelium is essential for epithelial-mesenchymal transition and breast cancer progression. *The Journal of clinical investigation* **121**, 1064-1074, doi:10.1172/JCI44540 (2011).

16 Yae, T. *et al.* Alternative splicing of CD44 mRNA by ESRP1 enhances lung colonization of metastatic cancer cell. *Nature communications* **3**, 883, doi:10.1038/ncomms1892 (2012).

17 Sacchetti, A. *et al.* Phenotypic plasticity underlies local invasion and distant metastasis in colon cancer. *Elife* **10**, doi:10.7554/eLife.61461 (2021).

18 Yang, Y. *et al.* Determination of a Comprehensive Alternative Splicing Regulatory Network and Combinatorial Regulation by Key Factors during the Epithelial-to-Mesenchymal Transition. *Molecular and cellular biology* **36**, 1704-1719, doi:10.1128/MCB.00019-16 (2016).

19 Nieto, M. A., Huang, R. Y., Jackson, R. A. & Thiery, J. P. Emt: 2016. *Cell* **166**, 21-45, doi:10.1016/j.cell.2016.06.028 (2016).

20 Dobin, A. *et al.* STAR: ultrafast universal RNA-seq aligner. *Bioinformatics* **29**, 15-21, doi:10.1093/bioinformatics/bts635 (2013).

21 Katz, Y., Wang, E. T., Airoldi, E. M. & Burge, C. B. Analysis and design of RNA sequencing experiments for identifying isoform regulation. *Nature Methods* **7**, 1009-1015, doi:10.1038/nmeth.1528 (2010).

22 Guinney, J. *et al.* The consensus molecular subtypes of colorectal cancer. *Nature medicine* **21**, 1350-1356, doi:10.1038/nm.3967 (2015).

23 Liberzon, A. *et al.* The Molecular Signatures Database (MSigDB) hallmark gene set collection. *Cell systems* **1**, 417-425, doi:10.1016/j.cels.2015.12.004 (2015).

24 Preca, B. T. *et al.* A self-enforcing CD44s/ZEB1 feedback loop maintains EMT and stemness properties in cancer cells. *Int J Cancer* **137**, 2566-2577, doi:10.1002/ijc.29642 (2015).

25 Cook, K. B., Kazan, H., Zuberi, K., Morris, Q. & Hughes, T. R. RBPDB: a database of RNA-binding specificities. *Nucleic Acids Res* **39**, D301-308, doi:10.1093/nar/gkq1069 (2011).

26 Schafer, S. *et al.* Alternative Splicing Signatures in RNA-seq Data: Percent Spliced in (PSI). *Current protocols in human genetics* **87**, 11 16 11-11 16 14, doi:10.1002/0471142905.hg1116s87 (2015).

27 Hernandez-Martinez, R., Ramkumar, N. & Anderson, K. V. p120-catenin regulates WNT signaling and EMT in the mouse embryo. *Proc Natl Acad Sci U S A* **116**, 16872-16881, doi:10.1073/pnas.1902843116 (2019).

28 Shimada, H. *et al.* The Roles of Tricellular Tight Junction Protein Angulin-1/Lipolysis-Stimulated Lipoprotein Receptor (LSR) in Endometriosis and Endometrioid-Endometrial Carcinoma. *Cancers (Basel)* **13**, doi:10.3390/cancers13246341 (2021).

29 Conway, J., Al-Zahrani, K. N., Pryce, B. R., Abou-Hamad, J. & Sabourin, L. A. Transforming growth factor beta-induced epithelial to mesenchymal transition requires the Ste20-like kinase SLK independently of its catalytic activity. *Oncotarget* **8**, 98745-98756, doi:10.18632/oncotarget.21928 (2017).

30 Karve, K., Netherton, S., Deng, L., Bonni, A. & Bonni, S. Regulation of epithelial-mesenchymal transition and organoid morphogenesis by a novel TGFbeta-TCF7L2 isoform-specific signaling pathway. *Cell Death Dis* **11**, 704, doi:10.1038/s41419-020-02905-z (2020).

31 Orian-Rousseau, V. CD44 Acts as a Signaling Platform Controlling Tumor Progression and Metastasis. *Frontiers in immunology* **6**, 154, doi:10.3389/fimmu.2015.00154 (2015).

32 Pece, S., Confalonieri, S., P, R. R. & Di Fiore, P. P. NUMB-ing down cancer by more than just a NOTCH. *Biochimica et biophysica acta* **1815**, 26-43, doi:10.1016/j.bbcan.2010.10.001 (2011).

33 Todaro, M. *et al.* CD44v6 is a marker of constitutive and reprogrammed cancer stem cells driving colon cancer metastasis. *Cell Stem Cell* **14**, 342-356, doi:10.1016/j.stem.2014.01.009 (2014).

34 Adam, R. A. & Adam, Y. G. Malignant ascites: past, present, and future. *Journal of the American College of Surgeons* **198**, 999-1011, doi:10.1016/j.jamcollsurg.2004.01.035 (2004).

35 Goswami, S. *et al.* Identification of invasion specific splice variants of the cytoskeletal protein Mena present in mammary tumor cells during invasion in vivo. *Clinical & experimental metastasis* **26**, 153-159, doi:10.1007/s10585-008-9225-8 (2009).

36 Varga, J. & Greten, F. R. Cell plasticity in epithelial homeostasis and tumorigenesis. *Nature cell biology* **19**, 1133-1141, doi:10.1038/ncb3611 (2017).

37 Dixit, A. *et al.* Perturb-Seq: Dissecting Molecular Circuits with Scalable Single-Cell RNA Profiling of Pooled Genetic Screens. *Cell* **167**, 1853-1866 e1817, doi:10.1016/j.cell.2016.11.038 (2016).

38 Lengauer, C., Kinzler, K. W. & Vogelstein, B. Genetic instability in colorectal cancers. *Nature* **386**, 623-627, doi:10.1038/386623a0 (1997).

899 39 Warzecha, C. C., Sato, T. K., Nabet, B., Hogenesch, J. B. & Carstens, R. P. ESRP1 and ESRP2 are
900 epithelial cell-type-specific regulators of FGFR2 splicing. *Molecular cell* **33**, 591-601,
901 doi:10.1016/j.molcel.2009.01.025 (2009).
902 40 Tavanez, J. P. & Valcarcel, J. A splicing mastermind for EMT. *EMBO J* **29**, 3217-3218,
903 doi:10.1038/emboj.2010.234 (2010).
904 41 Warzecha, C. C. *et al.* An ESRP-regulated splicing programme is abrogated during the epithelial-
905 mesenchymal transition. *EMBO J* **29**, 3286-3300, doi:10.1038/emboj.2010.195 (2010).
906 42 Calon, A. *et al.* Stromal gene expression defines poor-prognosis subtypes in colorectal cancer.
907 *Nat Genet* **47**, 320-329, doi:10.1038/ng.3225 (2015).
908 43 Isella, C. *et al.* Stromal contribution to the colorectal cancer transcriptome. *Nat Genet* **47**, 312-
909 319, doi:10.1038/ng.3224 (2015).
910 44 Pillman, K. A. *et al.* miR-200/375 control epithelial plasticity-associated alternative splicing by
911 repressing the RNA-binding protein Quaking. *EMBO J* **37**, doi:10.15252/embj.201899016 (2018).
912 45 Kim, E. J. *et al.* QKI, a miR-200 target gene, suppresses epithelial-to-mesenchymal transition and
913 tumor growth. *Int J Cancer* **145**, 1585-1595, doi:10.1002/ijc.32372 (2019).
914 46 Brabletz, S. & Brabletz, T. The ZEB/miR-200 feedback loop--a motor of cellular plasticity in
915 development and cancer? *EMBO Rep* **11**, 670-677, doi:10.1038/embor.2010.117 (2010).
916 47 Rokavec, M., Kaller, M., Horst, D. & Hermeking, H. Pan-cancer EMT-signature identifies RBM47
917 down-regulation during colorectal cancer progression. *Sci Rep* **7**, 4687, doi:10.1038/s41598-017-
918 04234-2 10.1038/s41598-017-04234-2 [pii] (2017).
919 48 Xia, R. M., Liu, T., Li, W. G. & Xu, X. Q. RNA-binding protein RBM24 represses colorectal
920 tumourigenesis by stabilising PTEN mRNA. *Clin Transl Med* **11**, e383, doi:10.1002/ctm2.383
921 (2021).
922 49 Lin, G. *et al.* RNA-binding Protein MBNL2 regulates Cancer Cell Metastasis through MiR-182-
923 MBNL2-AKT Pathway. *J Cancer* **12**, 6715-6726, doi:10.7150/jca.62816 (2021).
924 50 Zhang, J. *et al.* The natural compound neobractatin inhibits tumor metastasis by upregulating
925 the RNA-binding-protein MBNL2. *Cell Death Dis* **10**, 554, doi:10.1038/s41419-019-1789-5 (2019).
926 51 Lu, Z. X. *et al.* Transcriptome-wide landscape of pre-mRNA alternative splicing associated with
927 metastatic colonization. *Mol Cancer Res* **13**, 305-318, doi:10.1158/1541-7786.MCR-14-0366
928 (2015).
929 52 Xiao, H. MiR-7-5p suppresses tumor metastasis of non-small cell lung cancer by targeting NOVA2.
930 *Cell Mol Biol Lett* **24**, 60, doi:10.1186/s11658-019-0188-3 (2019).

53 Zeilstra, J. *et al.* Deletion of the WNT target and cancer stem cell marker CD44 in Apc(Min/+) mice attenuates intestinal tumorigenesis. *Cancer Res* **68**, 3655-3661, doi:10.1158/0008-5472.CAN-07-2940 (2008).

54 Zeilstra, J. *et al.* Stem cell CD44v isoforms promote intestinal cancer formation in Apc(min) mice downstream of Wnt signaling. *Oncogene* **33**, 665-670, doi:10.1038/onc.2012.611 (2014).

55 Misra, S., Hascall, V. C., De Giovanni, C., Markwald, R. R. & Ghatak, S. Delivery of CD44 shRNA/nanoparticles within cancer cells: perturbation of hyaluronan/CD44v6 interactions and reduction in adenoma growth in Apc Min/+ MICE. *J Biol Chem* **284**, 12432-12446, doi:10.1074/jbc.M806772200 (2009).

56 Orian-Rousseau, V., Chen, L., Sleeman, J. P., Herrlich, P. & Ponta, H. CD44 is required for two consecutive steps in HGF/c-Met signaling. *Genes Dev* **16**, 3074-3086, doi:10.1101/gad.242602 (2002).

57 Zhang, H. *et al.* CD44 splice isoform switching determines breast cancer stem cell state. *Genes Dev* **33**, 166-179, doi:10.1101/gad.319889.118 (2019).

58 Azevedo, R. *et al.* CD44 glycoprotein in cancer: a molecular conundrum hampering clinical applications. *Clinical proteomics* **15**, 22, doi:10.1186/s12014-018-9198-9 (2018).

59 Ponta, H., Sherman, L. & Herrlich, P. A. CD44: from adhesion molecules to signalling regulators. *Nature reviews. Molecular cell biology* **4**, 33-45, doi:10.1038/nrm1004 (2003).

Figure 1

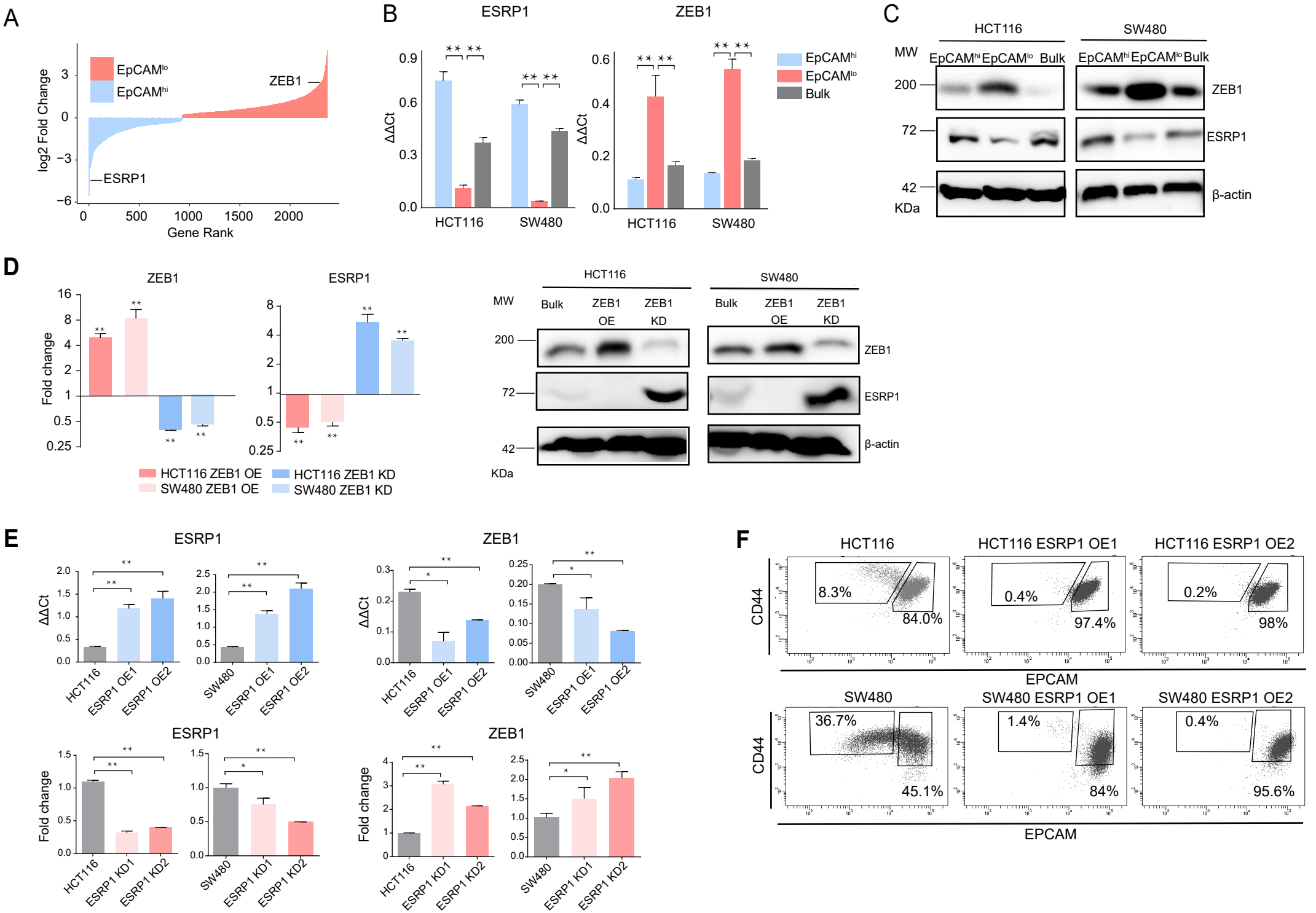
A
EpCAMlo
EpCAMhi
ZEB1
ESRP1
log2 Fold Change
Gene Rank
B
ESRP1
ZEB1
ΔΔCt
HCT116
SW480
EpCAMhi
EpCAMlo
Bulk
C
HCT116
SW480
MW
EpCAMhi EpCAMlo Bulk
EpCAMhi EpCAMlo Bulk
200
72
42
KDa
ZEB1
ESRP1
β-actin
D
ZEB1
ESRP1
Fold change
HCT116 ZEB1 OE
SW480 ZEB1 OE
HCT116 ZEB1 KD
SW480 ZEB1 KD
HCT116
SW480
MW
Bulk
ZEB1 OE
ZEB1 KD
200
72
42
KDa
ZEB1
ESRP1
β-actin
E
ESRP1
ZEB1
ΔΔCt
HCT116
ESRP1 OE1
ESRP1 OE2
SW480
ESRP1 KD1
ESRP1 KD2
Fold change
F
HCT116
HCT116 ESRP1 OE1
HCT116 ESRP1 OE2
SW480
SW480 ESRP1 OE1
SW480 ESRP1 OE2
CD44
EPCAM
8.3%
84.0%
0.4%
97.4%
0.2%
98%
36.7%
45.1%
1.4%
84%
0.4%
95.6%

Figure 2

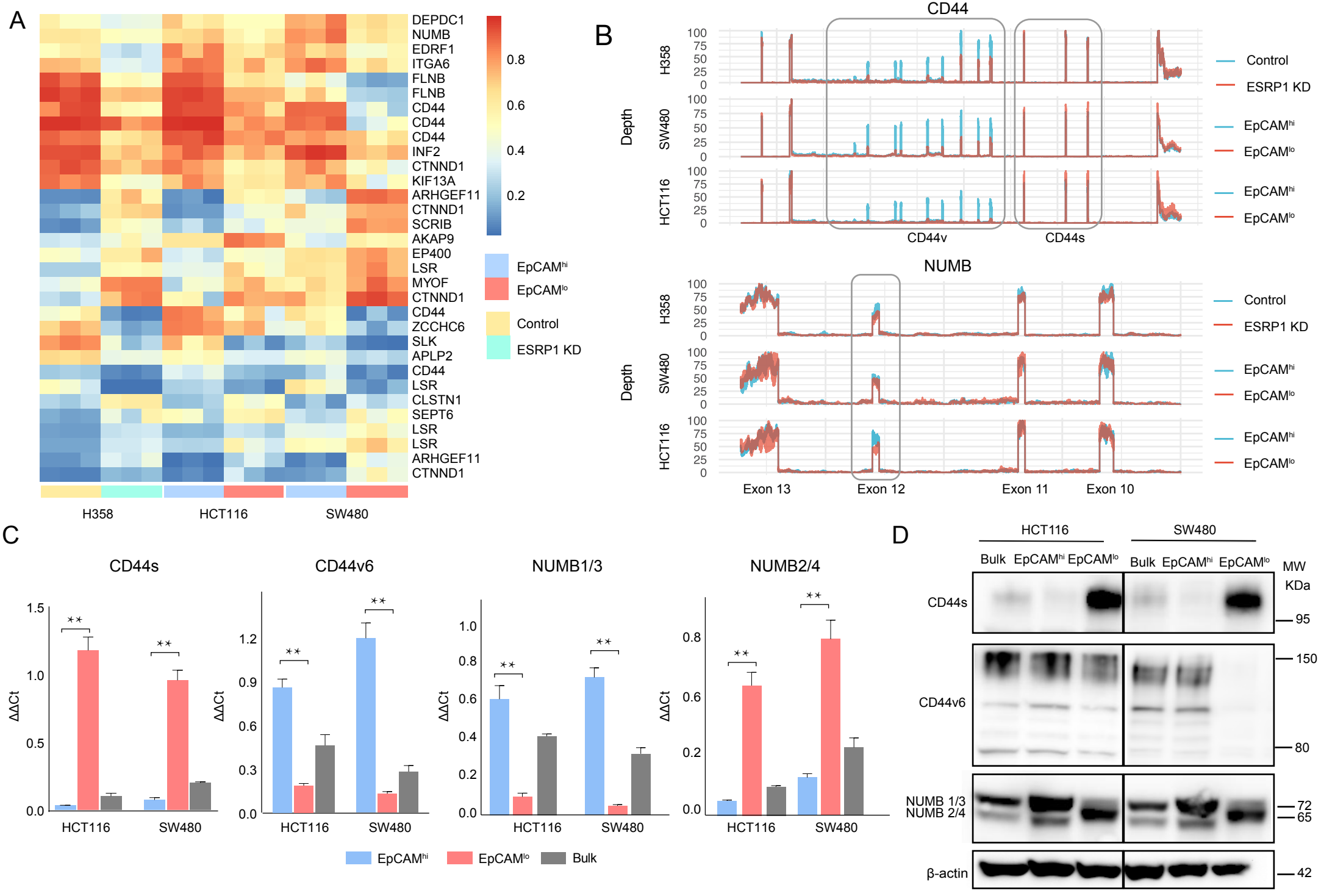
A
DEPDC1
NUMB
EDRF1
ITGA6
FLNB
FLNB
CD44
CD44
CD44
INF2
CTNND1
KIF13A
ARHGEF11
CTNND1
SCRIB
AKAP9
EP400
LSR
MYOF
CTNND1
CD44
ZCCHC6
SLK
APLP2
CD44
LSR
CLSTN1
SEPT6
LSR
LSR
ARHGEF11
CTNND1
0.8
0.6
0.4
0.2
EpCAMhi
EpCAMlo
Control
ESRP1 KD
H358
HCT116
SW480
B
CD44
NUMB
Depth
H358
SW480
HCT116
100
75
50
25
0
Control
ESRP1 KD
EpCAMhi
EpCAMlo
CD44v
CD44s
Exon 13
Exon 12
Exon 11
Exon 10
C
CD44s
CD44v6
NUMB1/3
NUMB2/4
ΔΔCt
**
HCT116
SW480
EpCAMhi
EpCAMlo
Bulk
D
HCT116
SW480
Bulk
EpCAMhi
EpCAMlo
MW
KDa
CD44s
CD44v6
NUMB 1/3
NUMB 2/4
β-actin
95
150
80
72
65
42

Figure 3

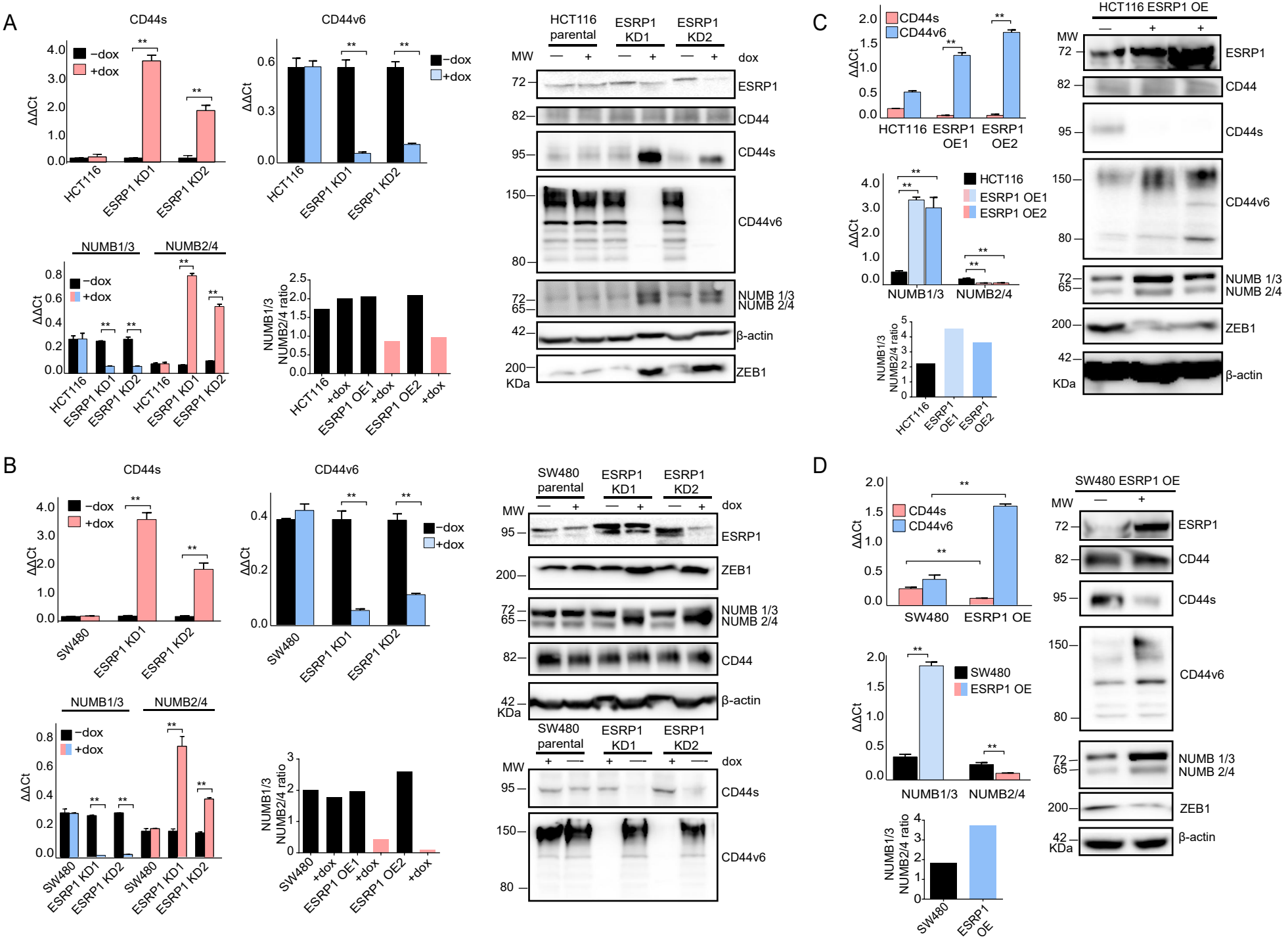
A
CD44s
CD44v6
−dox
+dox
ΔΔCt
HCT116
ESRP1 KD1
ESRP1 KD2
NUMB1/3
NUMB2/4
NUMB1/3 NUMB2/4 ratio
ESRP1 OE1
ESRP1 OE2
HCT116 parental
ESRP1 KD1
ESRP1 KD2
MW
dox
ESRP1
CD44
CD44s
CD44v6
NUMB 1/3
NUMB 2/4
β-actin
ZEB1
KDa
B
SW480
SW480 parental
C
HCT116 ESRP1 OE
D
SW480 ESRP1 OE

Figure 4

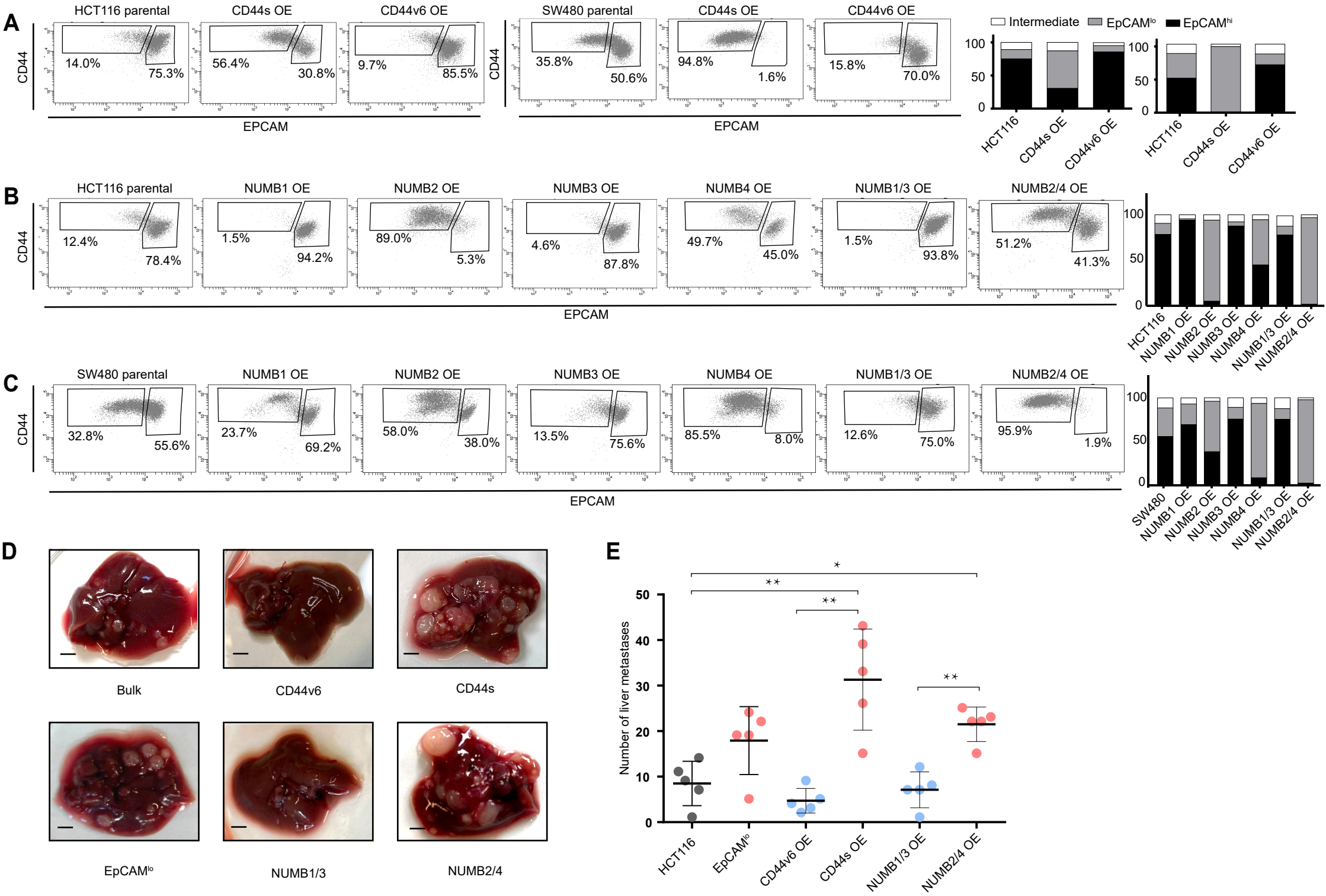
A
HCT116 parental
CD44s OE
CD44v6 OE
SW480 parental
CD44s OE
CD44v6 OE
CD44
EPCAM
14.0%
75.3%
56.4%
30.8%
9.7%
85.5%
35.8%
50.6%
94.8%
1.6%
15.8%
70.0%
Intermediate
EpCAMlo
EpCAMhi
HCT116
CD44s OE
CD44v6 OE
B
HCT116 parental
NUMB1 OE
NUMB2 OE
NUMB3 OE
NUMB4 OE
NUMB1/3 OE
NUMB2/4 OE
12.4%
78.4%
1.5%
94.2%
89.0%
5.3%
4.6%
87.8%
49.7%
45.0%
1.5%
93.8%
51.2%
41.3%
C
SW480 parental
32.8%
55.6%
23.7%
69.2%
58.0%
38.0%
13.5%
75.6%
85.5%
8.0%
12.6%
75.0%
95.9%
1.9%
D
Bulk
CD44v6
CD44s
EpCAMlo
NUMB1/3
NUMB2/4
E
Number of liver metastases
HCT116
EpCAMlo
CD44v6 OE
CD44s OE
NUMB1/3 OE
NUMB2/4 OE

Figure 5

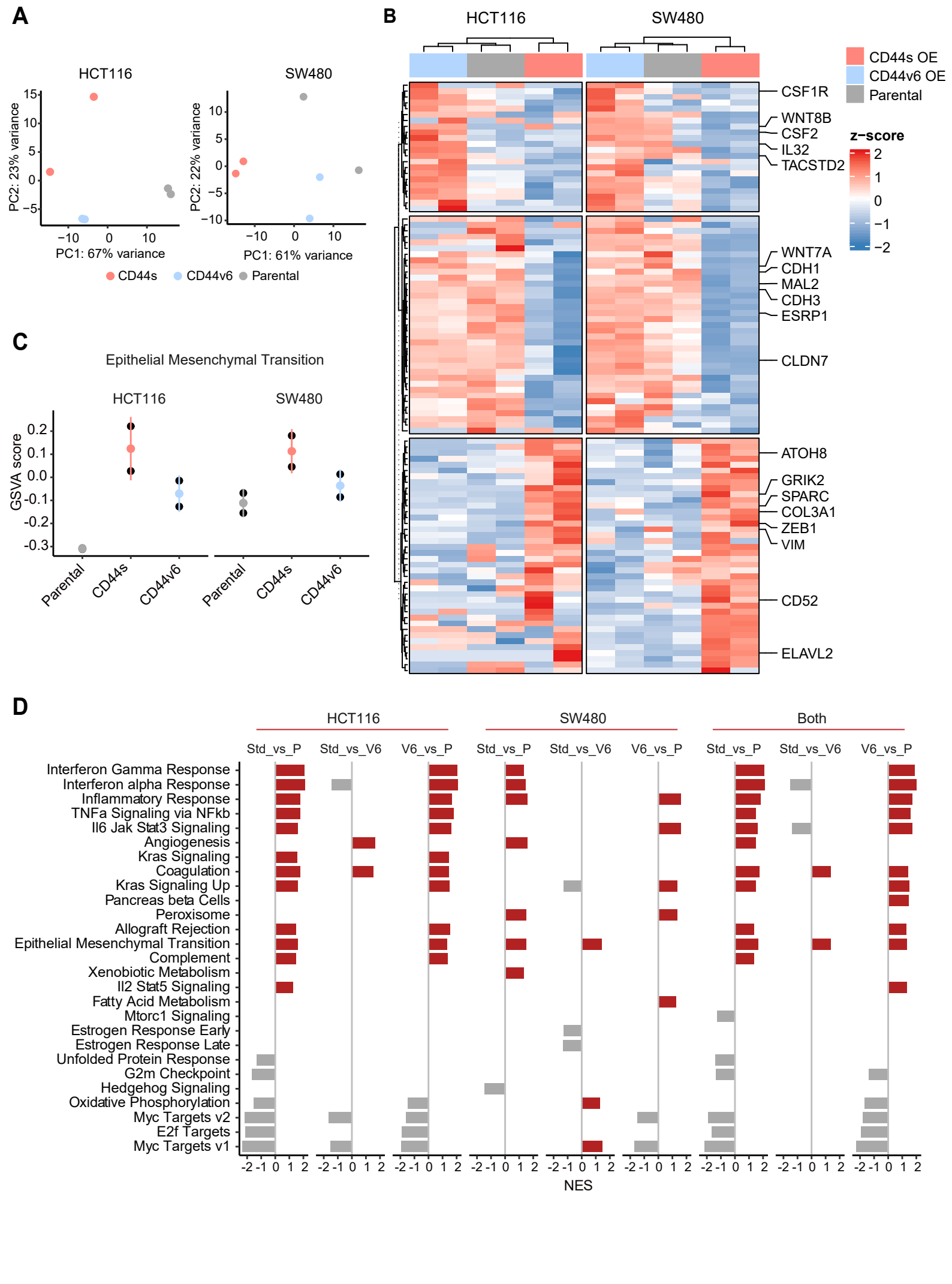
A
HCT116
SW480
PC2: 23% variance
PC2: 22% variance
PC1: 67% variance
PC1: 61% variance
CD44s
CD44v6
Parental
B
HCT116
SW480
CD44s OE
CD44v6 OE
Parental
z-score
CSF1R
WNT8B
CSF2
IL32
TACSTD2
WNT7A
CDH1
MAL2
CDH3
ESRP1
CLDN7
ATOH8
GRIK2
SPARC
COL3A1
ZEB1
VIM
CD52
ELAVL2
C
Epithelial Mesenchymal Transition
HCT116
SW480
GSVA score
Parental
CD44s
CD44v6
D
HCT116
SW480
Both
Std_vs_P
Std_vs_V6
V6_vs_P
Interferon Gamma Response
Interferon alpha Response
Inflammatory Response
TNFa Signaling via NFkb
Il6 Jak Stat3 Signaling
Angiogenesis
Kras Signaling
Coagulation
Kras Signaling Up
Pancreas beta Cells
Peroxisome
Allograft Rejection
Epithelial Mesenchymal Transition
Complement
Xenobiotic Metabolism
Il2 Stat5 Signaling
Fatty Acid Metabolism
Mtorc1 Signaling
Estrogen Response Early
Estrogen Response Late
Unfolded Protein Response
G2m Checkpoint
Hedgehog Signaling
Oxidative Phosphorylation
Myc Targets v2
E2f Targets
Myc Targets v1
NES

Figure 6

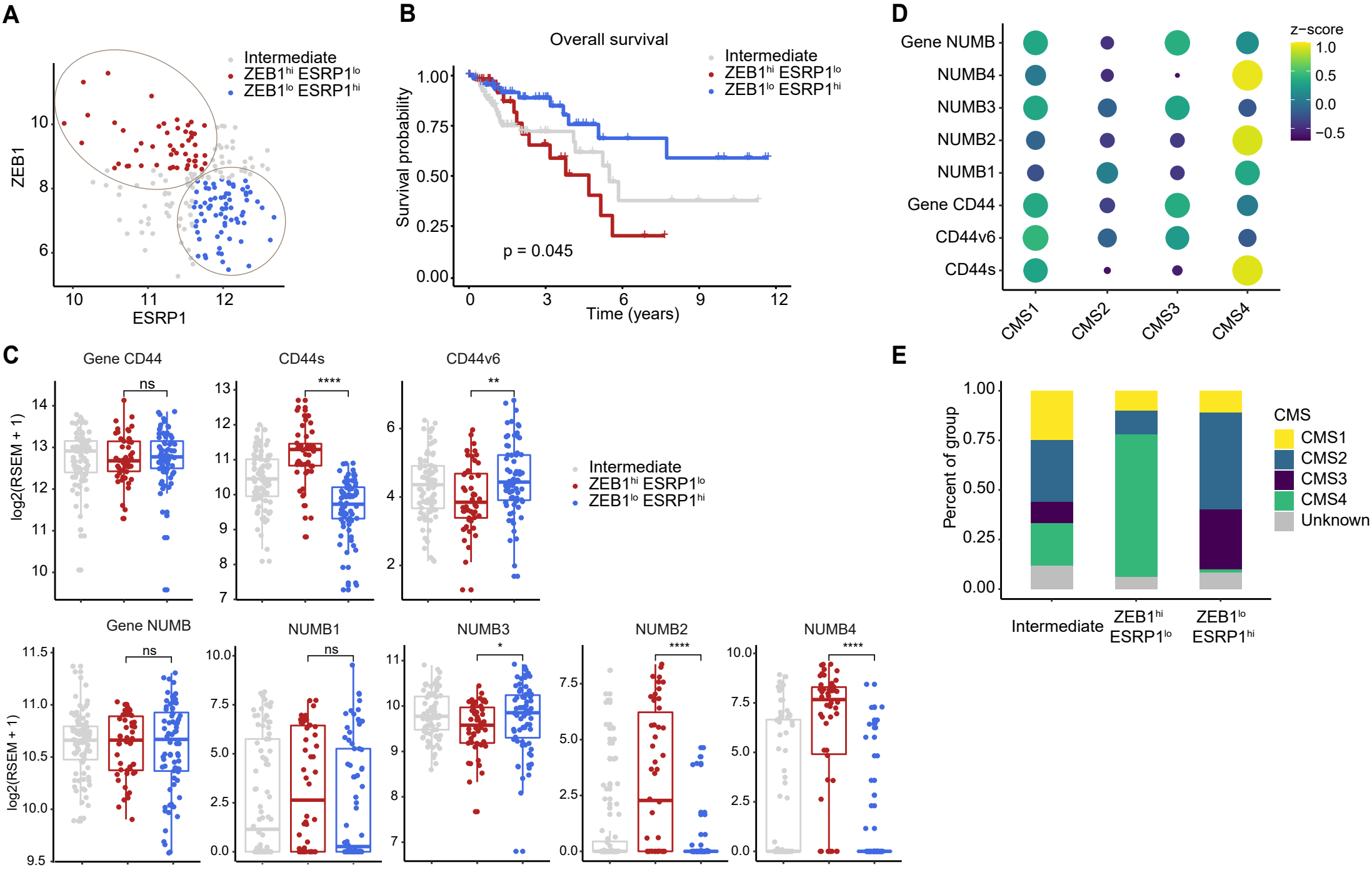
A
Intermediate
ZEB1hi ESRP1lo
ZEB1lo ESRP1hi
ZEB1
ESRP1
B
Overall survival
Survival probability
p = 0.045
Time (years)
C
Gene CD44
CD44s
CD44v6
Gene NUMB
NUMB1
NUMB3
NUMB2
NUMB4
log2(RSEM + 1)
ns
D
Gene NUMB
NUMB4
NUMB3
NUMB2
NUMB1
Gene CD44
CD44v6
CD44s
z−score
CMS1
CMS2
CMS3
CMS4
E
Percent of group
CMS
Unknown
Intermediate

Figure 7

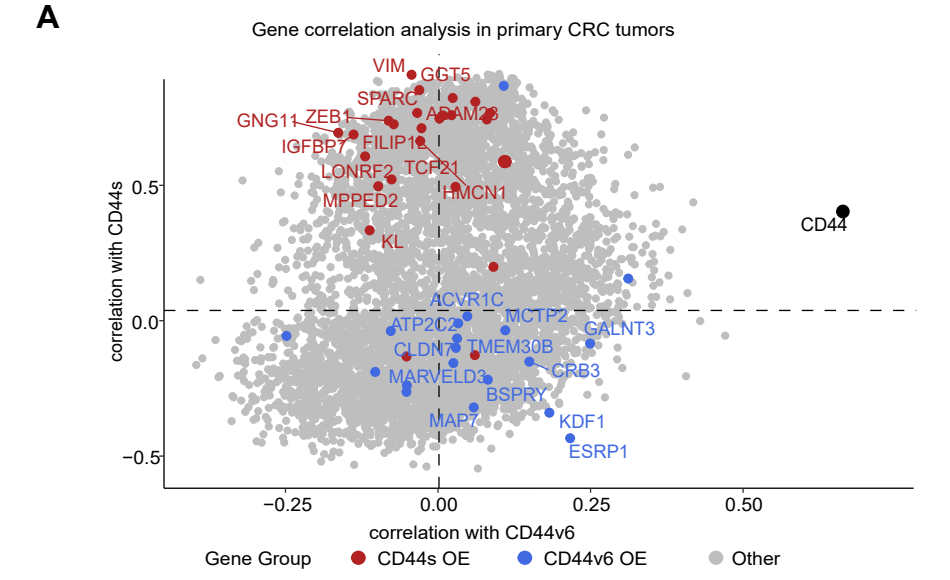
A
Gene correlation analysis in primary CRC tumors
VIM
GGT5
SPARC
ADAM23
GNG11
ZEB1
IGFBP7
FILIP1L
LONRF2
TCF21
HMCN1
MPPED2
KL
CD44
ACVR1C
MCTP2
ATP2C2
GALNT3
CLDN7
TMEM30B
MARVELD3
CRB3
BSPRY
MAP7
KDF1
ESRP1
correlation with CD44s
0.5
0.0
−0.5
−0.25
0.00
0.25
0.50
correlation with CD44v6
Gene Group
CD44s OE
CD44v6 OE
Other

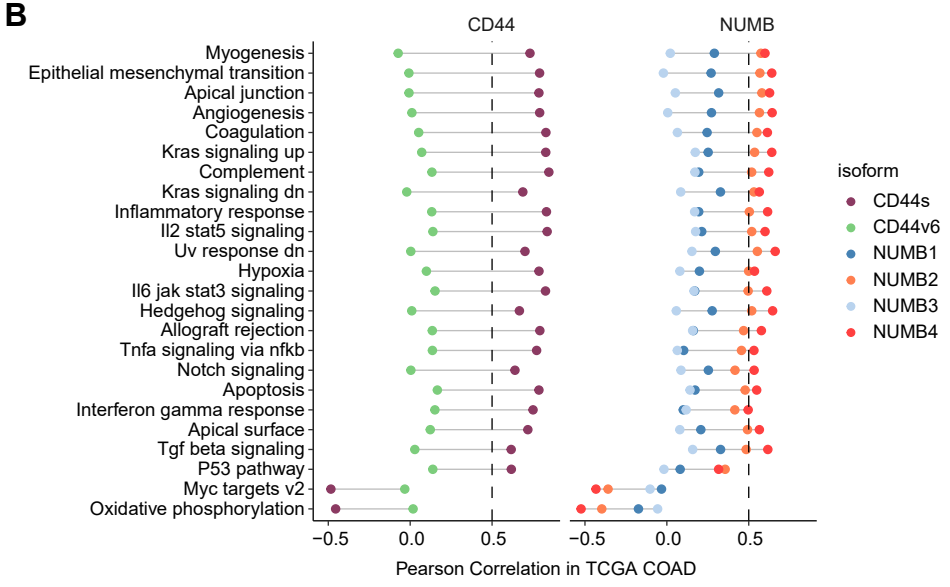
B
CD44
NUMB
Myogenesis
Epithelial mesenchymal transition
Apical junction
Angiogenesis
Coagulation
Kras signaling up
Complement
Kras signaling dn
Inflammatory response
Il2 stat5 signaling
Uv response dn
Hypoxia
Il6 jak stat3 signaling
Hedgehog signaling
Allograft rejection
Tnfa signaling via nfkb
Notch signaling
Apoptosis
Interferon gamma response
Apical surface
Tgf beta signaling
P53 pathway
Myc targets v2
Oxidative phosphorylation
−0.5
0.0
0.5
Pearson Correlation in TCGA COAD
isoform
CD44s
CD44v6
NUMB1
NUMB2
NUMB3
NUMB4

Figure 1- figure supplement 1

A

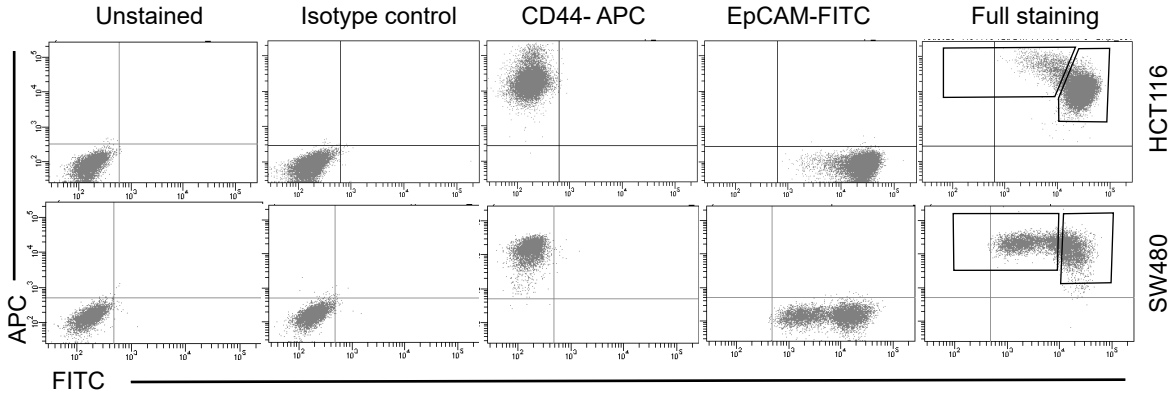

B

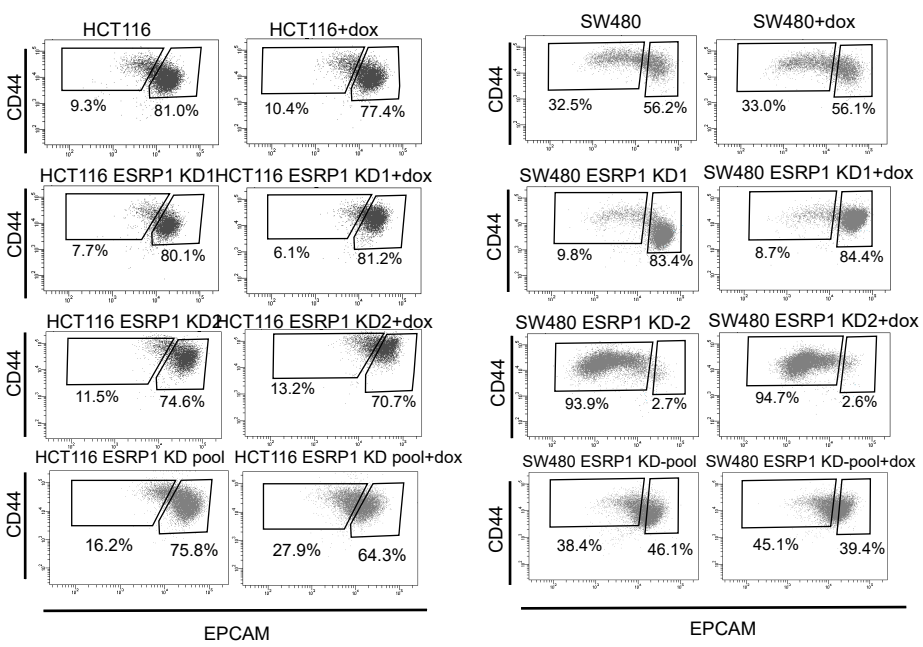

C

Gene Name	log2FC_HCT116	log2FC_SW480
ESRP1	-2.22645	-6.89236
ESRP2	-0.896173	-1.89007
NOVA2	0.757111	2.2421
RBM47	-1.36442	-0.900345
MBNL2	0.784795	0.355627
MBNL3	-0.637449	-2.0392
RBM24	1.52564	NS
RBM19	-0.496814	NS
HNRNPAB	-0.452521	NS
HNRNPF	-0.352169	NS
RBM43	0.490142	NS
U2AF2	-0.385724	NS
RBM14	NS	-0.458869
QKI	NS	0.643307
SRSF5	NS	0.412868
HNRNPH1	NS	0.244149

D

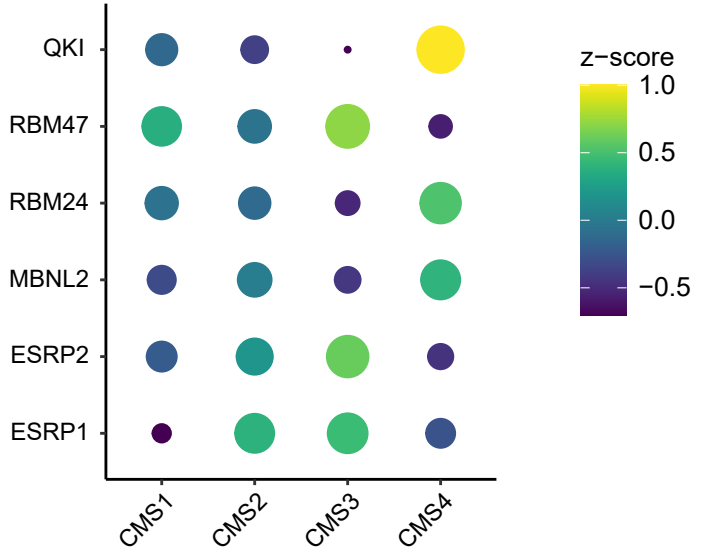

Figure 2- figure supplement 1

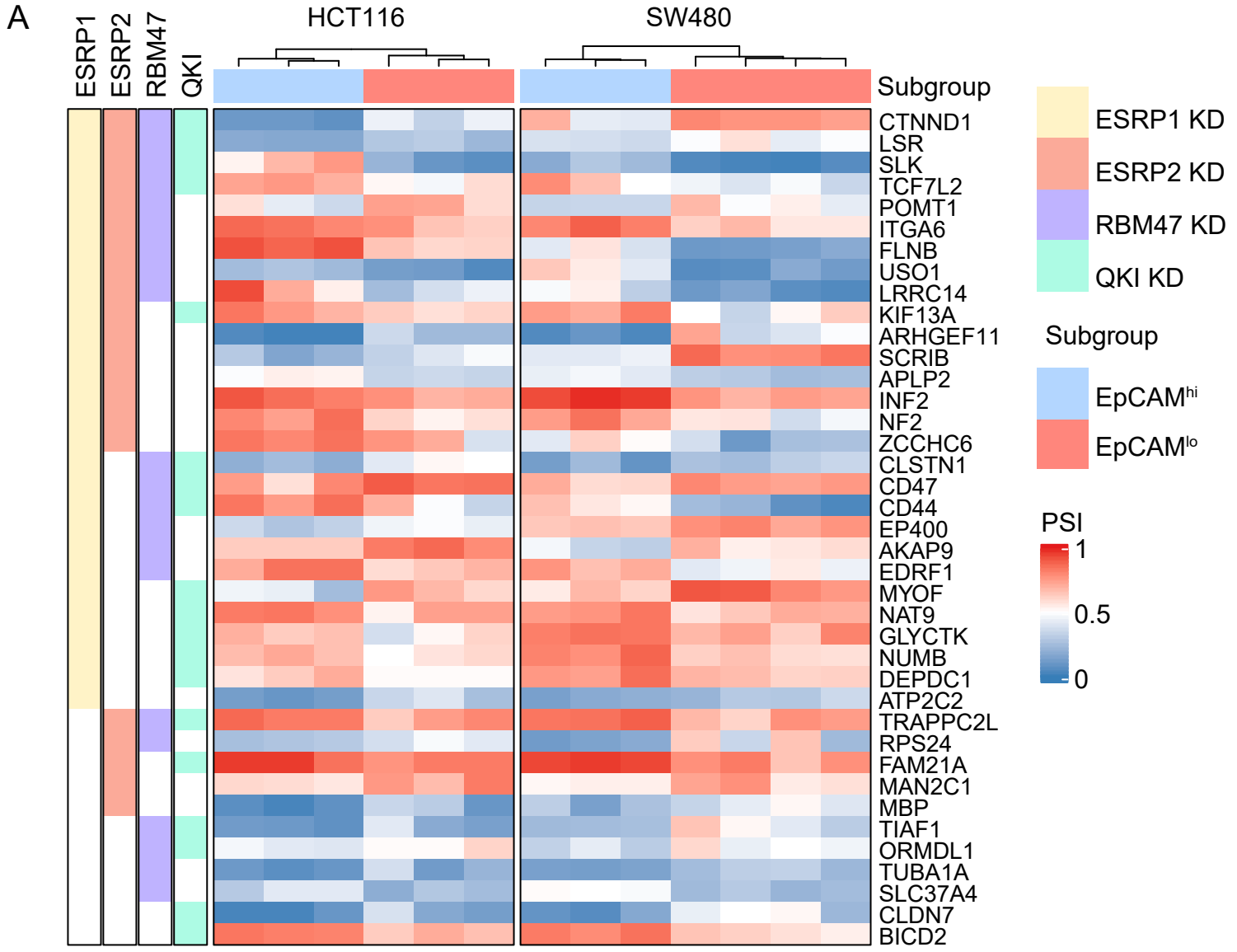

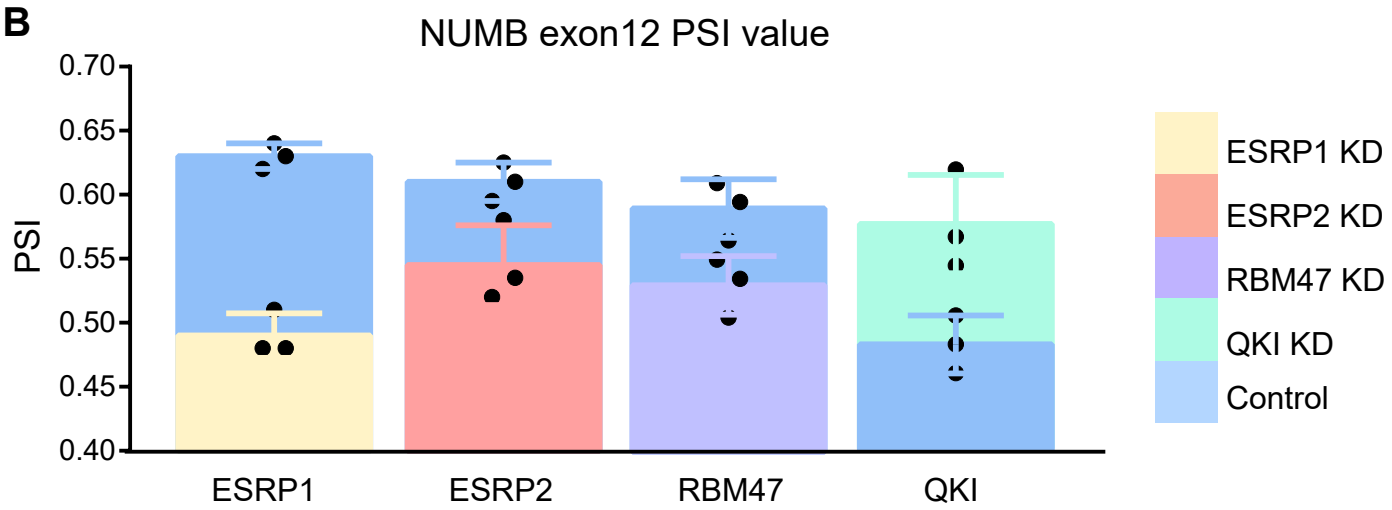

Figure 3- figure supplement 1

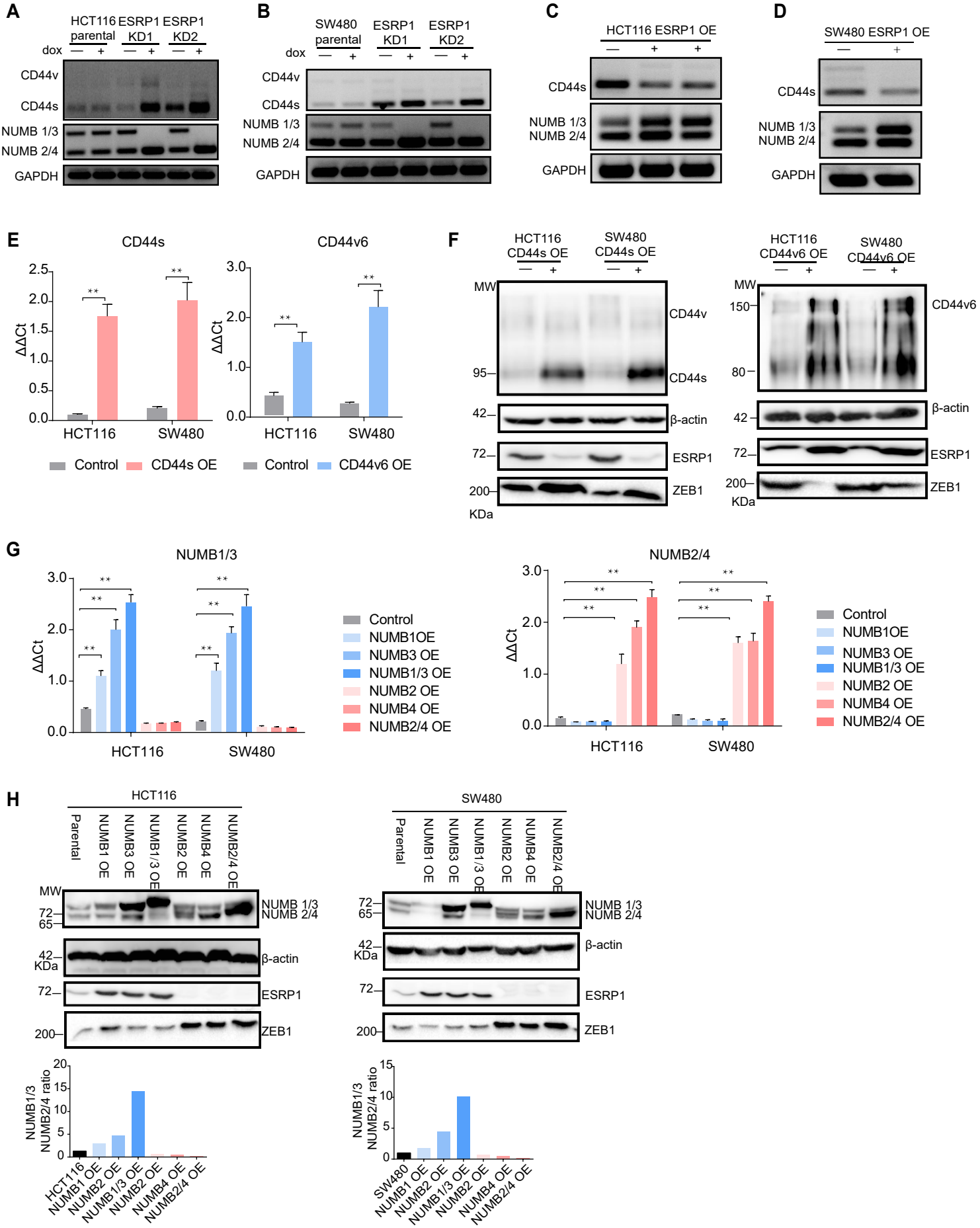

Figure 3- figure supplement 2

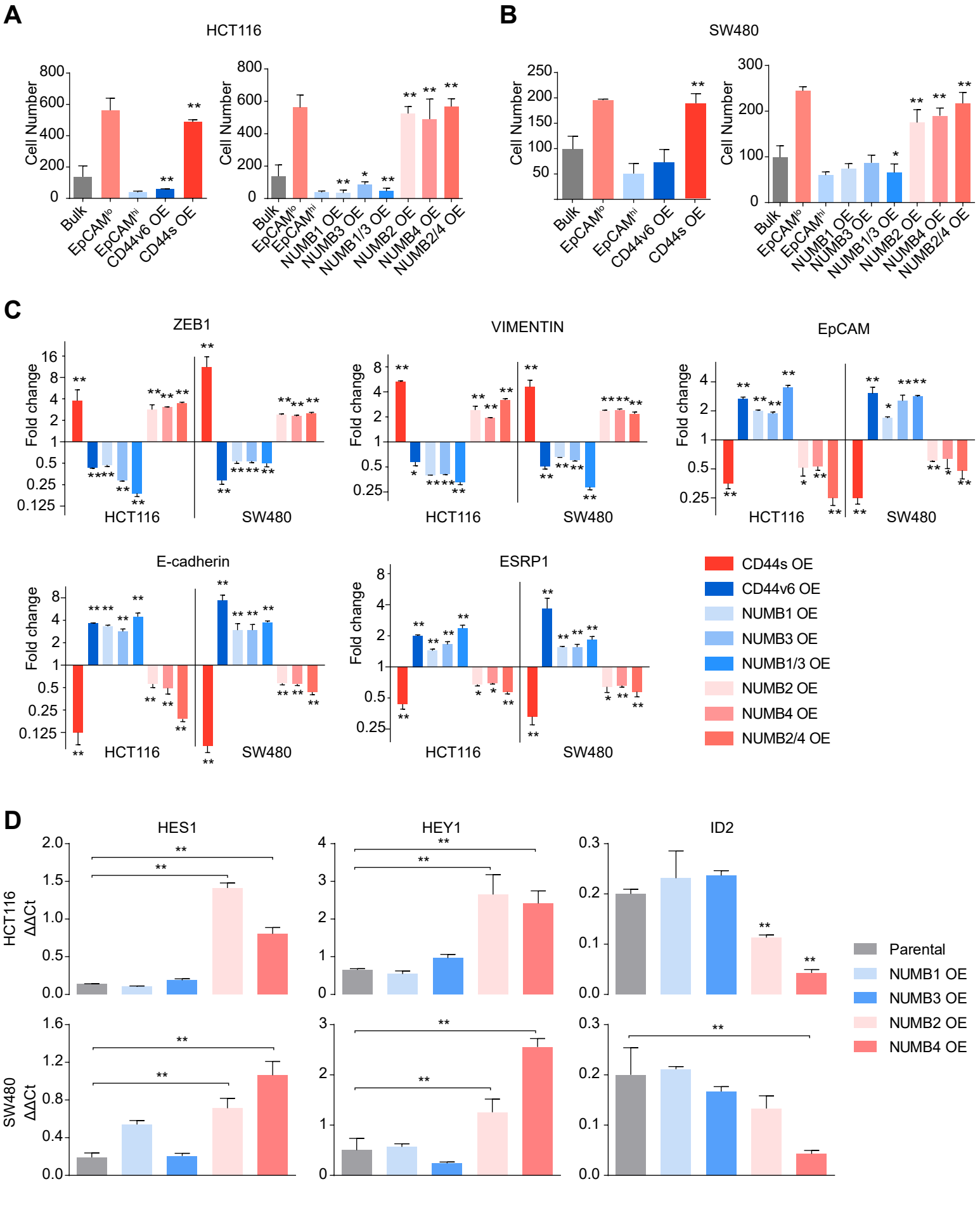

Figure 4- figure supplement 1

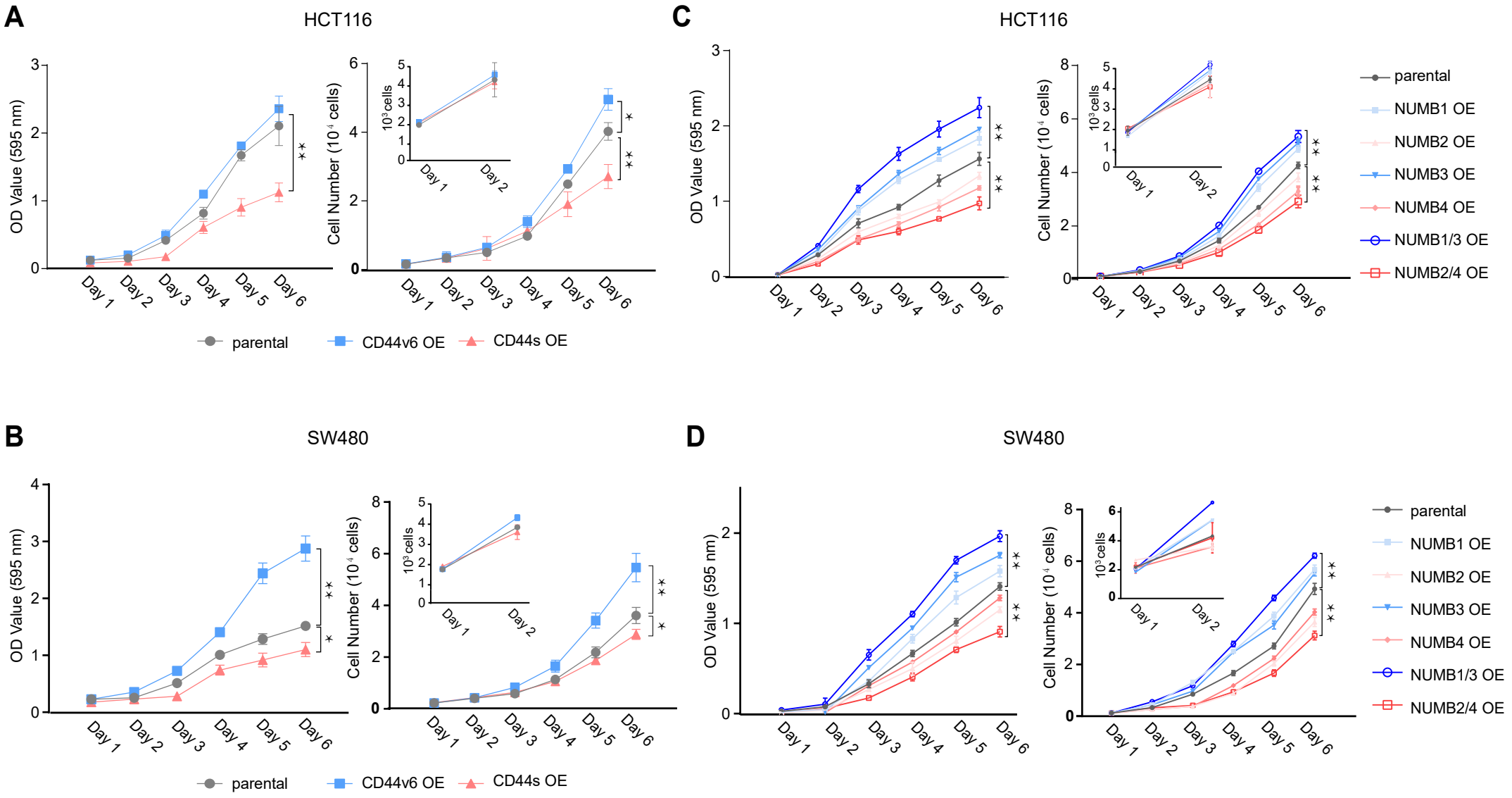

Figure 5- figure supplement 1

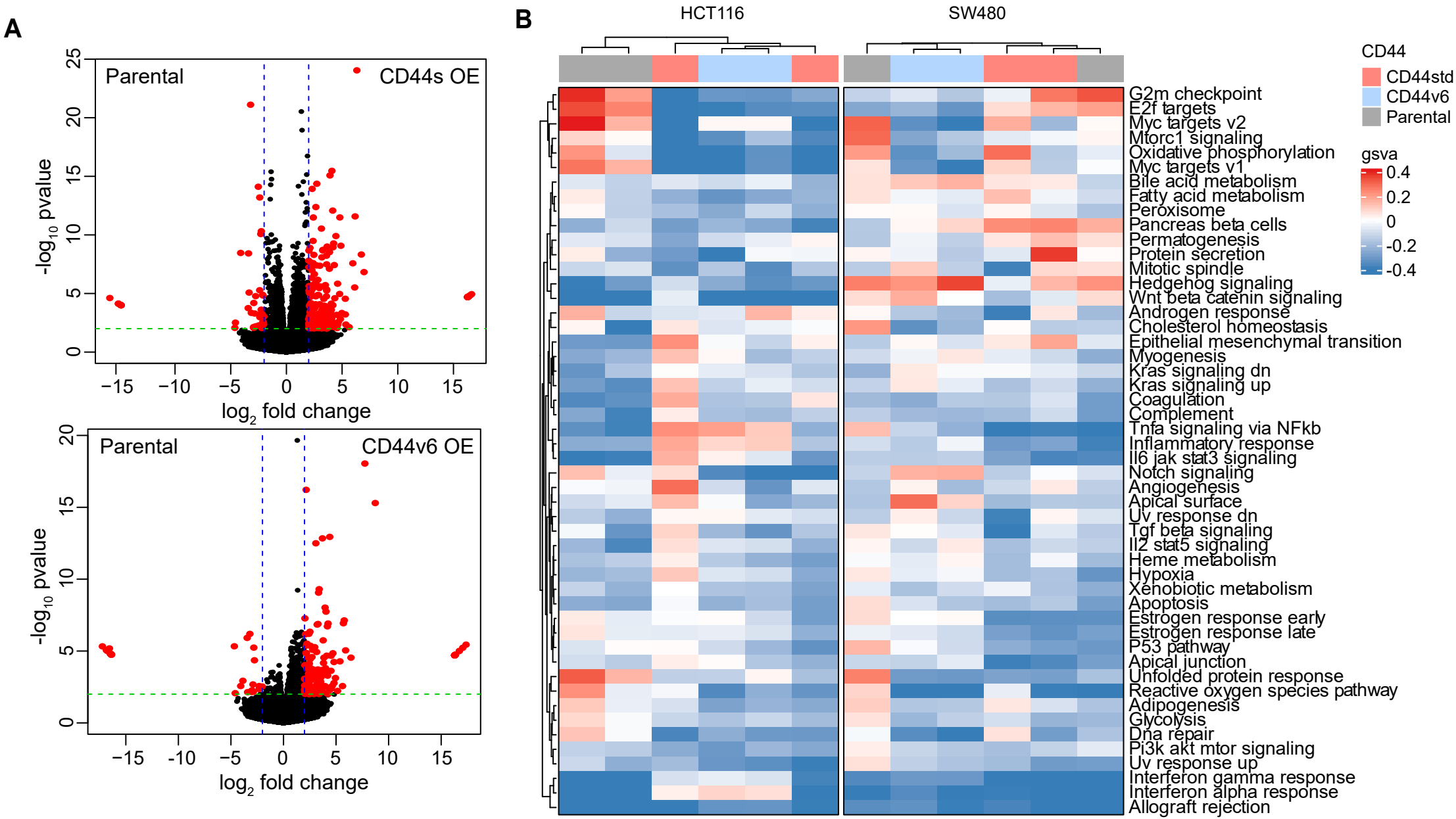

Figure 7- figure supplement 1